Conf-9109332--4

NEW APPROACHES TO STUDIES OF EXOTIC NUCLEI

CONF-9109332--4

DE92 010127

J. H. HAMILTON

Department of Physics and Astronomy
Vanderbilt University, Nashville, TN 37235 (USA)

Proceedings, International School of Nuclear Physics: 4π High Resolution Gamma Ray Spectroscopy, Erice, Italy, September 20-28, 1991, to be published in Progress in Particles and Nuclear Physics

ABSTRACT

New generations of 4π gamma-ray detectors, recoil mass spectrometers (RMS), and radioactive beam accelerators will open up many new areas of research, including presently inaccessible in-beam and radioactive decay studies of exotic nuclei still farther off stability. The new generation RMS and radioactive beam developments at the Holifield Heavy Ion Research Facility are presented. Current research and future prospects to probe the N = Z line up to ^{100}Sn are described. Superdeformation in A = 70 to 190 nuclei is described in terms of its underlying physics of reinforcing proton and neutron shell gaps which lead to new superdeformed, doubly-magic nuclei. Recent results provide new insights into the coexistence of multiple nuclear shapes near the ground states.

INTRODUCTION

Nuclear structure and low energy heavy ion physics are experiencing an exciting resurgence brought on by the development of very powerful new experimental facilities with sensitivities three to five orders of magnitude (10^3-10^5) greater than those currently available along with new theoretical developments which can treat unexplored regions and have predicted new phenomena like hyperdeformed nuclei with 3:1 axis ratios and deformations $\beta_2 \sim 1.0$! These powerful new facilities under development include 4π gamma-ray detector arrays with 50 to 100 and more, much higher efficiency Compton suppressed Ge detectors such as GAMMASPHERE in the U.S. and EUROGAM and EUROBALL in Europe and new generation recoil mass separators specifically for nuclear structure studies at Oak Ridge and recently completed for studies of fragmentation products at GSI and Michigan State. The design and power of the new generation RMS at Oak Ridge are described in this paper, and new 4π detector systems are described in other papers in these proceedings. The new physics which can be addressed by the use of accelerated beams of radioactive isotopes have captured our imagination, as documented in the proceedings of recent international conferences at Berkeley, 1989, Los Alamos, 1990, and Belgium, 1991. The proposed Oak Ridge Exotic Beam (OREB) facility, which can quickly (2 yrs.) and inexpensively (~$4M) open many new windows is described. Indeed, radioactive ion beams (RIB) in combination with the new generation 4π detectors and RMS's can open exciting new windows to view our universe, from the structure of nuclei to energy production in stars to how the elements were formed in nucleosynthesis.

Current research and future prospects to extend our understandings of nuclei along the N = Z line are presented. The underlying physics which gives nuclei superdeformation with $\beta_2 \sim 0.4$ and $\beta_2 \sim 0.6$ through the reinforcement of the proton and neutron shell gaps when they have the same deformation is discussed. New insights into the coexistence of multiple shapes with different deformations in nuclei have been found in the A = 30,70,100,120 and 180 regions. Recent, more microscopic theoretical calculations in the Excited FED VAMPIR (Variation After Mean-Field Projection In Realistic model spaces) are found to be remarkably successful in explaining the new complexity of shape coexisting level structures in ^{68}Ge. The importance of electric monopole, E0, mode in probing the coexistence of different structures is expanding into odd-A as well as even-even nuclei and into new regions as seen in recent UNISOR work on ^{120}Ba. Additional exciting recent discoveries can be found in a recent overview of the properties of nuclei in and near their ground states (Hamilton 1991).

SUPERDEFORMATION AND ITS UNDERLYING PHYSICS OF REINFORCING PROTON AND NEUTRON SHELL GAPS

Our discovery of a new region of ground state superdeformation with axis ratio of 3:2 and $\beta_2 \sim 0.4$ in ^{74,76}Kr (Hamilton 1981; Piercey et al., 1981) and our analysis of the data in the superdeformed region around $^{80,100}_{38}Sr_{60,62}$ (refs. Kahn et al., 1977; Azuma et al., 1979) led to an understanding of the physics underlying these two new islands of ground state superdeformation as well as of the more recently discovered regions of superdeformation at high spins in the mass 152 region (Twin et al., 1986), 130 region (Kirwan et al., 1987) and 190 region (Moore et al., 1989); namely, that there must be shell gaps in the single particle levels at the same superdeformation, $\beta_2 \sim$ 0.4 or 0.6 for both protons and neutrons so that the protons and neutrons reinforce each other for a nucleus to be superdeformed (Hamilton 1981; Hamilton 1985a,b, 1991).

Superdeformation in nuclei continues to be the focus of much attention in nuclear structure physics. Superdeformed prolate nuclei fall into two groups with simple ratios of their long to short axis: Group 1 with 3:2 axis ratios and deformations, $\beta_2 \sim 0.4$-0.45, and Group 2 with 2:1 axis ratios with $\beta_2 \sim 0.6$. In Table 1 the regions where superdeformed states are observed are given. Although most of the attention has been given to superdeformation at high spin following the discovery of a high spin superdeformed band in ^{152}Dy (Twin et al., 1986), note that superdeformation had been discovered in nuclei in and near their ground states long before as shown in Table 1.

The opening up of this field began with Strutinsky's (1967a, b) interpretation of the fission isomers in the actinide elements as a shell structure effect which produced a second minimum in the potential at $\beta_2 \sim 0.6$. Bjørnholm and Lynn (1982) have reviewed this field. It was many years before more direct evidence for these superdeformed minima were obtained. Recently Schirmer et al. (1989) established the excitation energy of 2.75 ± 0.01 MeV for the 0^+ state in the superdeformed minimum for ^{236m}U by γ-decay to the ground state with the Heidelberg-Darmstadt Crystal Ball in the reaction ^{235}U(d,p).

Historically, the next observation of superdeformation was for an excited band in ^{72}Se, which crosses the near-spherical ground state band at low (2-4) spin (Hamilton et al., 1974, 1976). However, the superdeformed character of this band was not appreciated until after our work on ^{74,76}Kr. The next reference to this phenomena was the ISOLDE discovery of superdeformation in the ^{100}Sr ground state (Azuma et al., 1979). At that time, this was interpreted as arising from the neutron shell gap at $\beta \sim 0.4$ for N = 60. Next came the discovery of superdeformation in the ground states of ^{74,76}Kr (Hamilton et al., 1986; Piercey et al., 1981). In these nuclei there is strong mixing between the superdeformed ground states and the excited near-spherical

Table 1. Regions where superdeformation have been discovered. The underlying physics involves the reinforcement of proton and neutron shell gaps for the same superdeformation to stabilize the superdeformation. The reinforcing shell gaps responsible for the superdeformation are shown.

Mass Region	Discovery Year	States	Reinforcing Deformed Shell Gaps
	Nuclei With 3:2 Axis Ratios, $\beta_2 \sim 0.4$		
A ~ 100	1979	Ground States	Z=38, N=60,62
A ~ 76	1981[a]	Ground States	Z=38, N=38
A ~ 130	1987	High Spin States	Z=58, N=72,74
A ~ 190	1989	High Spin States	Z=80, N=112,116
	Nuclei With 2:1 Axis Ratios, $\beta_2 \sim 0.6$		
A ~ 242	1967	Fission Isomers	Z=94, N=144,148
A ~ 150	1986	High Spin States	Z=64,66 N=84,86

[a]The first evidence in 1974 for excited states in ^{72}Se

band which coexist at low spin. If one scales the 2^+-0^+ unperturbed energies in ^{74}Kr and ^{100}Sr by $A^{5/3}$ for comparison with the previously known most deformed ground state in ^{240}Pu $E(2_1^+) = 43$ keV (as first done for ^{100}Sr), their 2_1 energies of 28 and 40 keV, respectively, are much lower to indicate their superdeformed character.

From an analysis of the level structures of their neighboring nuclei, these new superdeformed nuclei were found to occur in islands of superdeformation which were produced by the protons and neutrons having shell gaps at the same $\beta_2 \sim 0.4$ to reinforce each other (Hamilton 1981, 1985). The islands were proposed (Hamilton 1981, 1985) to be centered on nuclei with shell gaps at the same deformation $\beta_2 \sim 0.4$ for both protons and neutrons, so reinforcement occurs for Z = N = 38 and Z = 38, N = 60, 62 (see Fig. 1). The importance of the shell gap reinforcement and not simply the N = 60 shell gap as first proposed as the origin of the superdeformation can be seen in Fig. 2. There one sees that the 2^+ energies rise sharply so the superdeformation disappears quickly for N = 60 as Z moves away from 38 as noted earlier in developing this understanding. Subsequent work confirmed ^{76}Sr as the center of this island (Varley et al., 1987). Independently, the calculations of Möller and Nix (1981a,b) predicted the island of superdeformation centered around Z = N = 38.

Recently we extended the levels of $^{72}_{34}Se_{38}$ to 26^+ (Chaturvedi et al., 1991), Fig. 3, where now one sees the very regular spacings of the gamma ray energies as characteristic of superdeformation. In the mass 130, 150 and 190 regions much effort has been given to finding the weakly (1-5%) populated superdeformed bands from which no connections to any known yrast state have been observed. By contrast, in ^{72}Se the superdeformed band is connected to the near-spherical ground band and is yrast by 4^+ above which it totally dominates the high spin state population in heavy ion reactions (Chaturvedi et al., 1991).

The reinforcement of the proton and neutron shell gaps for both spherical and deformed shapes can be understood from Fig. 1. We now can understand why 40 is a good spherical magic number so that $^{68}_{28}Ni_{40}$ and $^{90,96}_{40}Zr_{50,56}$ are spherical double magic closed shell nuclei like $^{16}_{8}O_8$, $^{40,48}_{20}Ca_{20,28}$ and $^{208}_{82}Pb_{126}$, and $^{88}_{38}Sr_{50}$ is nearly so. For both N and Z, 40 is spherical magic when it is reinforced by a strong spherical shell gap like 28 and 50 or even a moderately strongly spherical subshell gap at 56. However, we discovered (Hamilton 1981; Piercey et al., 1981) that as both Z and N approach 38,40 there is a switch in importance from the spherical gaps at N = Z = 40 (and 38) to the gaps at $\beta_2 \sim 0.4$ for Z = N = 38 dominating. So, $^{76}_{38}Sr_{38}$ in its ground

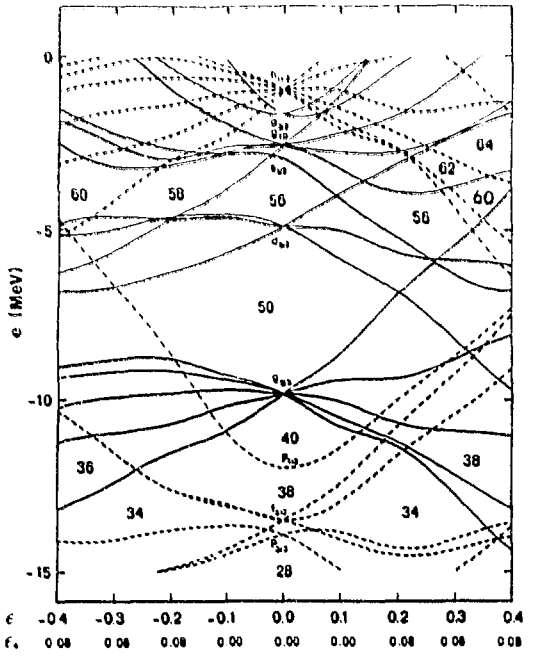

Fig. 1. Single particle levels as a function of deformation.

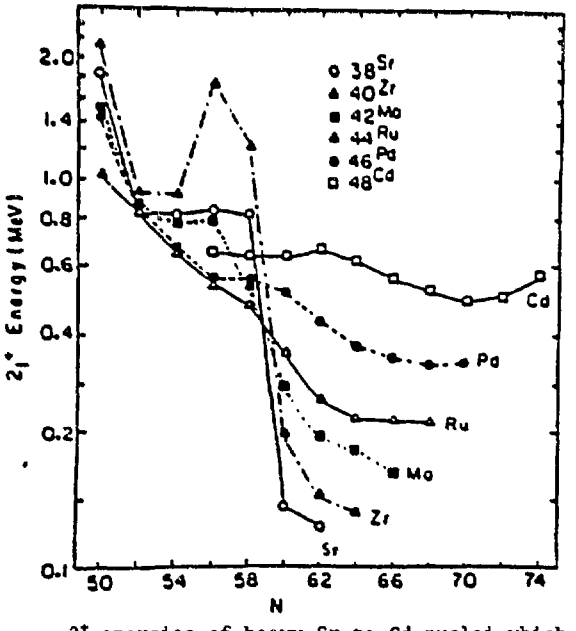

Fig. 2. 2_1^+ energies of heavy Sr to Cd nuclei which show the sudden onset of large deformation for N = 60 only in Sr and Zr nuclei with Z = 38 and 40.

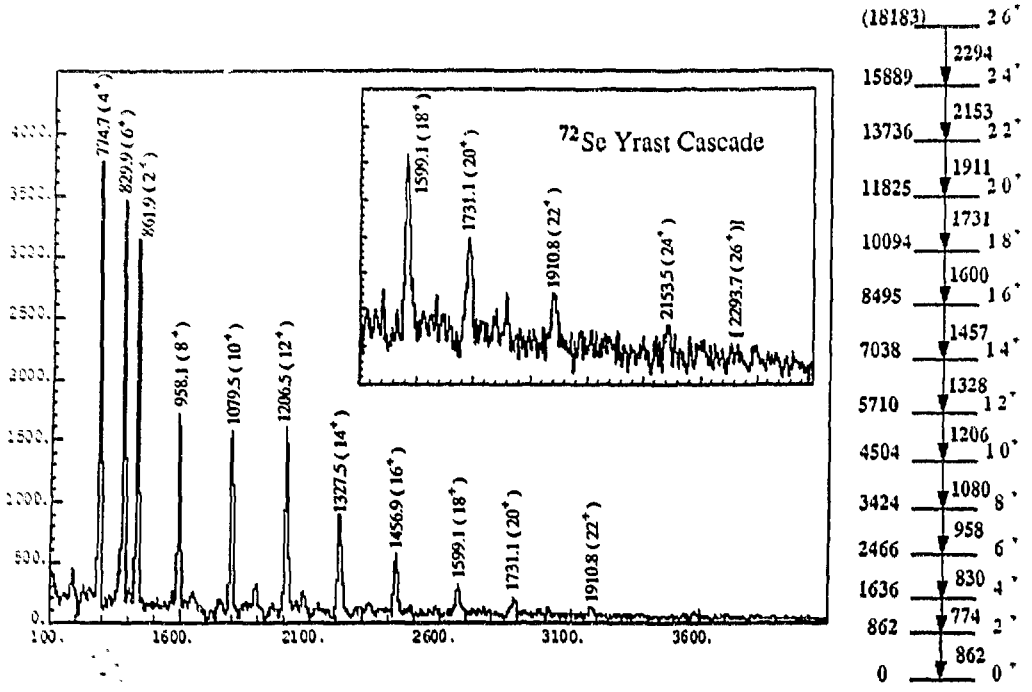

Fig. 3. The sum gate on the yrast cascade in ^{72}Se (Chaturvedi et al., 1991)

state is a new superdeformed double magic nucleus, and a similar reinforcement for Z = 38, N = 60,62 make $^{98,100}_{38}Sr_{60,62}$ superdeformed double magic nuclei in their ground states, too (Hamilton 1981; Hamilton 1985a,b). Similarly, $^{152}_{66}Dy_{86}$ and $^{192}_{80}Hg_{112}$ are superdeformed double magic nuclei but only at high spins (Hamilton 1991, Janssens and Khoo 1991). The Z = 66, N = 86 reinforcing shell gaps at $\beta_2 \sim 0.6$ for ^{152}Dy and Z = 80, N = 112 reinforcing shell gaps at $\beta_2 \sim 0.4$-0.45 for ^{192}Hg are seen in Figs. 4 and 5. This understanding (Hamilton 1981; Hamilton 1985a,b, Hamilton 1991) of the importance of proton-neutron shell gap reinforcement to give stabilization to these superdeformed nuclear shapes across the periodic table in addition to stabilizing spherical shapes around spherical double magic $^4_2He_2$, $^{16}_8O_8$, $^{40,48}_{20}Ca_{20,28}$, and $^{208}_{82}Pb_{126}$ as predicted in the Mayer and Jansen spherical shell model is a significant advance in the nuclear shell model.

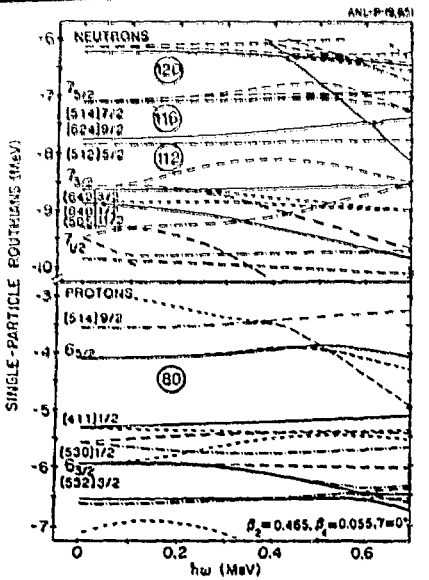

Fig. 4. Neutron and proton Woods-Saxon routhians for ^{192}Hg calculated for the deformation parameters β_2, β_4, and γ indicated. The orbitals are labeled by their asymptotic Nilsson quantum numbers $[Nn_3\Lambda]\Omega$ or, in the case of the high N intruder orbitals, by N_0. The conventions for labeling the orbitals are from Riley et al., (1990).

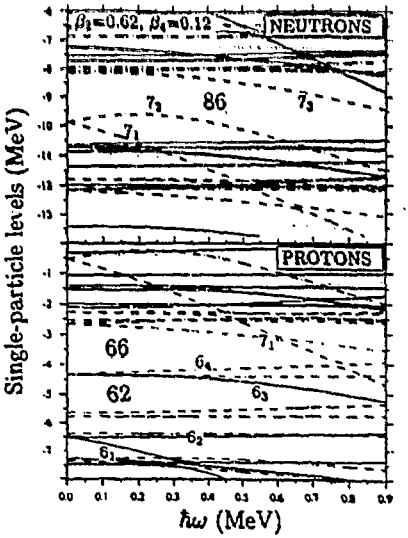

Fig. 5. WS single-particle superdeformed energies in the rotating frame vs. rotational frequency for neutrons and protons at the superdeformed minimum, $\beta_2 = 0.62$, $\beta_4 = 0.12$. The following line convention was used: solid (π = +, α = 1/2), dotted (+, -1/2), dot-dash (-, 1/2), and long-dashed (-, -1/2). The lowest high-N orbits, originating from the $i_{13/2}$(N = 6) and the $j_{15/2}$(N = 7) subshells, are indicated (Nazarewicz et al., 1989).

NEW INSIGHTS FROM EXTENDING OUR KNOWLEDGE ALONG THE N = Z LINE

For over 20 years since the first international conference on "How and Why to Study Nuclei Far From Stability", an important goal (Bergstrom 1966; Hamilton 1972) has been the extension of our knowledge of nuclei along the N = Z line to higher Z. However, only in the last five to six years have experimental facilities become available that have allowed us to significantly extend our knowledge with the discovery of levels in $^{64}_{32}$Ge to $^{84}_{42}$Mo (Ooi 1986; Görres et al., 1987; Varley et al., 1987; Lister et al. 1988; Lister et al., 1987; Golletly et al., 1991). Recent work on $^{84}_{42}$Mo where only one γ-ray, presumably the 2^+-0^+ transition, was weakly observed indicates that present facilities have reached their limit. However, further extension of the N = Z line to higher Z remains a very important goal as emphasized in the recent report of the Long Range Planning Committee of the U.S. Nuclear Science Advisory Committee in "Nuclei, Nucleons, Quarks: Nuclear Science in the 1990's":

> "The study of N = Z nuclei is particularly important. Such nuclei should have maximal interaction between protons and neutrons, and questions of the behavior of proton-neutron pairing can be answered by their systematic study."

One of the most important but undiscovered N = Z nucleus is $^{100}_{50}$Sn. This nucleus offers an opportunity to test the predictions of the spherical shell model that it should be a spherical double magic nucleus under extreme conditions of low proton to neutron ratio in a much higher Coulomb field. Indeed, one of the important justifications for the proposed Oak Ridge Exotic Beam (OREB) extension at the Holifield Heavy Ion Research Facility is that, "Detailed measurements of nuclear properties near the predicted double-closed shell nucleus, ^{100}Sn, will offer a stringent test of the microscopic independent-particle quantum structure that forms the foundation of the nuclear shell model" (Garrett and Olsen, 1991).

Now let us look at some of the new physics which has come out of recent searches for and identification of levels in $^{68}_{34}$Se to $^{84}_{42}$Mo and the insights into the experimental techniques which have guided the development of a new generation recoil mass spectrometer, RMS, and the proposed radioactive beam facility, OREB, at HHIRF. The RMS has been designed to open up studies of the structures of exotic products produced very far from stability with very low cross-sections, including new N = Z nuclei (Cormier et al, 1990). The OREB facility and the new generation RMS will be the most powerful system under consideration with capabilities to reach ^{100}Sn and beyond, as well as nuclei with even more protons than neutrons such as Tz = -1, $^{70}_{36}$Kr$_{34}$.

Following our discovery of superdeformation in the mass 70 region, extensive efforts were made by our group with the Rochester RMS and by a Daresbury group to identify ^{76}Sr to confirm its predicted (Hamilton 1985a,b) superdeformed shape. The Daresbury group succeeded in identifying levels in ^{76}Sr and confirming its superdeformation (Lister et al., 1988). They also identified levels in $^{68}_{34}$Se, $^{72}_{36}$Kr and $^{80}_{40}$Zr (Görres et al., 1987; Varley et al., 1987; Lister et al., 1987). At the Rochester RMS we could use only normal reactions (light projectile-heavy target) because the beam could not be separated sufficiently from the recoil products in an inverse reaction. At the Daresbury RMS, inverse reactions (heavy projectiles on a light target), like ^{24}Mg(^{54}Fe,2n)^{76}Sr and ^{16}O(^{58}Ni,2n)^{72}Kr were used. Inverse reactions make possible a Z identification gate from a ΔE detector as well as mass gate on the γ spectra. The counts as a functions of ΔE(Z) for mass 72 and RM-Z-γ spectra are shown in Fig. 6. The cross-sections for the production of these four N = Z nuclei are 10-60 μb, to make the N = Z products more than 10^3 smaller than the other products with the same mass. Only with a Z gate could transitions in these isotopes and the next N = Z nucleus $^{84}_{42}$Mo be identified. None of the new 4π detector arrays used without a RMS mass and Z gate could pick out in this region where the x-rays are low in energy the gamma rays associated with a 10-100 μb cross section nucleus.

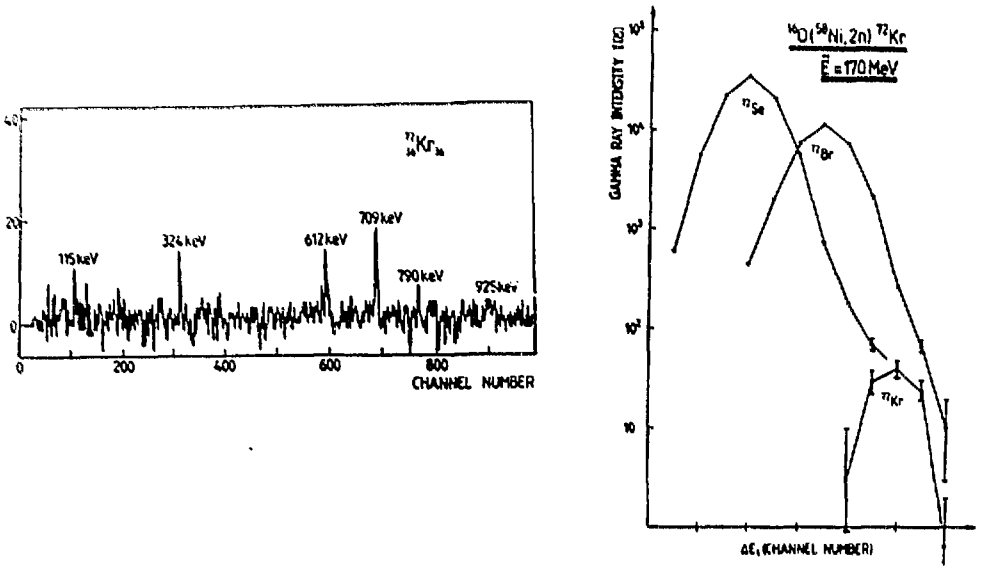

Fig. 6. The counts as a functions of ΔE(Z) for mass 72 and RM-Z-γ spectra.

As one looks in more detail at the single particle levels in the mass 70-100 region along the N = Z line shown in Fig. 7, one could expect a variety of different superdeformed structures such as oblate superdeformation in N = Z = 36, ^{72}Kr with β_2 ~ -0.4 and prolate superdeformation with β_2 ~ 0.5 for $^{84}_{42}Mo_{42}$ and β_2 ~ 0.6 (2:1 axis ratio for $^{88}_{44}Ru_{44}$, for example. In the RM-Z-γ spectrum of ^{84}Mo, Fig. 8, only one transition of 444 keV is seen weakly and is assigned as the 2^+_1-0^+ transition (Gelletly et al., 1991). Thus, ^{84}Mo seems to be the limit of the N = Z line that can be studied with the Daresbury RMS with 30 Ge detectors. The higher energy of 444 keV in ^{84} Mo compared to 290 keV for the 2^+-0^+ transition in $^{80}_{40}$Zr, as shown in Fig. 9, was interpreted (Gelletly et al., 1991) as evidence that deformation was significantly decreasing in ^{84}Mo as one moves farther from the N = Z = 38 shell gaps at β~ 0.4. This would mean that the N = Z = 42 shell gaps at β ~ 0.5 (Fig. 7) are not as important as the N = Z = 38 ones. This could be related to the fact that the N = Z = 50 spherical shell gaps are so dominating that already by N = Z = 42 they are making their domination felt. However, recall if only the $2^+ \rightarrow 0^+$ transitions of 456 and 424 keV in ^{74,76}Kr, respectively, had been observed, then one would not have suspected that the ground states of these nuclei are superdeformed with β ~ 0.4 (Hamilton et al. 1981; Piercey et al. 1981). The interaction between their ground state energies and low-lying near-spherical bands push the 0^+ ground state energies down and make their 2^+_1-0^+ energies look characteristic of more near-spherical nuclei. With only one gamma ray in ^{84}Mo, one cannot exclude this possibility of shape coexisting structures enlarging the 2^+ - 0^+ energy there, too. So, in fact, the influence of the N = Z = 42 shell gaps at β_2 ~ 0.5 (Fig. 7) and shape coexistence in ^{84}Mo remain open questions until more levels are seen.

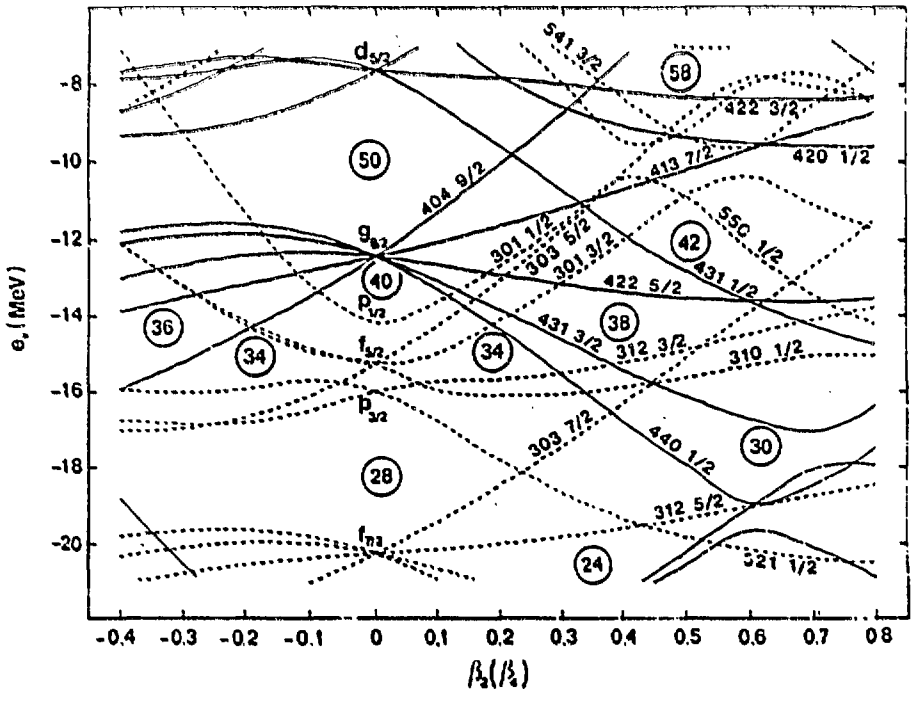

Fig. 7. Nilsson single-particle levels as functions of the quadrupole deformation β_2, calculated using the Woods-Saxon potential. Some particle numbers corresponding to large shell gaps are shown in circles (Nazarewicz et al., 1985).

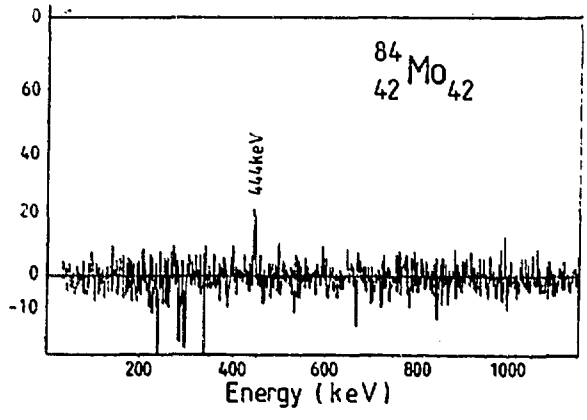

Fig. 8. RMS-Z-γ spectra of ^{84}Mo (Gelletly et al., 1991).

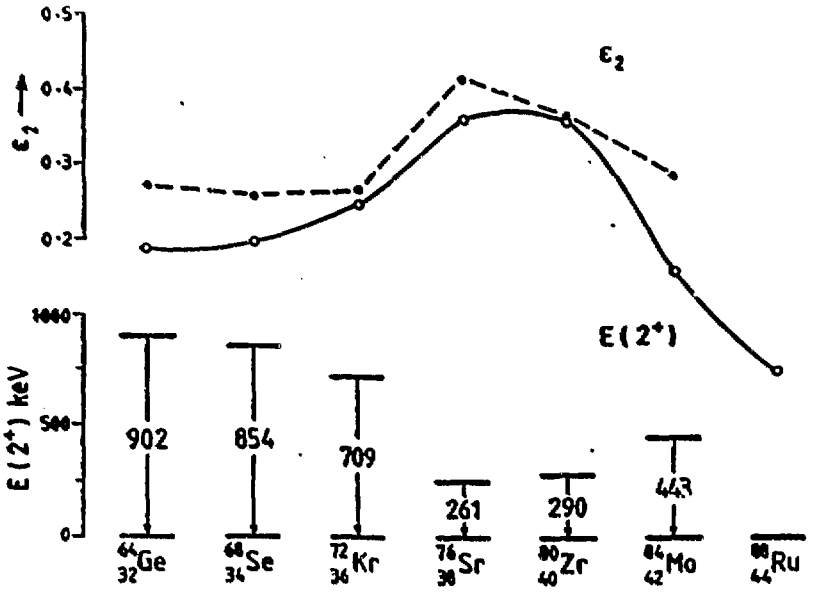

Fig. 9. The 2^+ energies for N = Z nuclei (Gelletly et al., 1991).

A second important insight comes out of ^{72}Kr studies (Varley et al., 1987; Dejbakhsh et al., 1990). From RMS-Z-γ singles data (Fig. 6), the 115 and 342 keV transitions were assigned to a side band with large deformation feeding the 709 keV 2_1^+ level, where the feeding transition out of the side band was the 115 keV transition. The 612, 790 and 925 keV transitions were assigned to depopulate the 4^+, 6^+ and 8^+ levels, respectively. After identifying for the first time gamma rays in ^{73}Kr (Satteson et al. 1990) with the Rochester RMS, we carried out a long γ-γ coincidence run at HHIRF. Some ^{72}Kr gamma rays also were observed in the γ-γ experiment. A gate on the 709 keV is shown in Fig. 10. The 612 keV transition is clearly seen, but the 115 and 342 keV gammas are not seen in the 709 keV gate (Dejbakhsh et al., 1990). So, the side band is not as placed (Varley et al., 1987). With the same analysis procedures as used earlier (Hamilton et al. 1981; Piercey et al. 1981), we noted there is a greater anomaly in the 2-0 energy in ^{72}Kr (a back bend in the J_1 moment of inertia) than in ^{74,76}Kr as seen in Fig. 11. The results of the analysis of $^{72-78}$Kr are shown in Table 2. Note the energy difference, ΔE_0, between the unperturbed (before interaction) energies of the 0^+ heads of the bands built on the two different shapes (for ^{74}Kr smaller deformation and superdeformation) changes sign between ^{72}Kr and the heavier isotopes to indicate the two bands have reversed positions. On the other hand, to have the same sign and magnitude for ΔE_0 for ^{72}Kr and ^{74}Kr would require a doubling of the interaction strength. Thus, a major change occurs in the ^{72}Kr ground state structure compared to the prolate superdeformation in ^{74,76}Kr (Dejbakhsh et al., 1990). New laser data show a sudden drop in mean square charge radius for ^{72}Kr compared to ^{74,76}Kr to confirm this change. So, it is possible that the ^{72}Kr ground state has a large oblate deformation, $\beta_2 \approx -0.4$, as could be expected from the reinforcement of the Z = N = 36 shell gaps seen in Fig. 7. If so, ^{72} Kr is an oblate deformed double

magic nucleus and its ground state interacts with an excited (presumably prolate) band to shift down the 0⁺ ground state energy. In some recent calculations, however, the excited band in ^{72}Kr is superdeformed with even larger $\beta_2 \sim 0.5$ while in ^{80}Zr an excited much less deformed band is predicted (Girod et al., 1990). This work (Dejbakhsh et al., 1990) clearly demonstrates the crucial importance of having γ-γ or RM-Z-γ-γ coincidences to place observed gamma rays in a level scheme and not simply RM-Z-γ spectra.

Table 2. Band mixing parameters in MeV for Kr isotopes.

Nucleus	δE	$E(0_2^+)$	ΔE_0 $E(0_2^+)^a - E(0_1^+)^a$	V
^{72}Kr	0.525	0.732[a]	+0.17 -0.318[a]	-0.66 0.330[a]
^{74}Kr[b]	0.256	0.681[a]	+0.169[a]	0.330[a]
^{76}Kr[b]	0.187	0.770	+0.396	0.330
^{78}Kr[b]	0.102	1.017	+0.813	0.305

[a]The value of the interaction strength, V, is assumed and $E(0_2^+)$ and ΔE_0 are calculated by using this value.

[b]The values for these nuclei are taken from the work of R. B. Piercey et al. (1981, 1982).

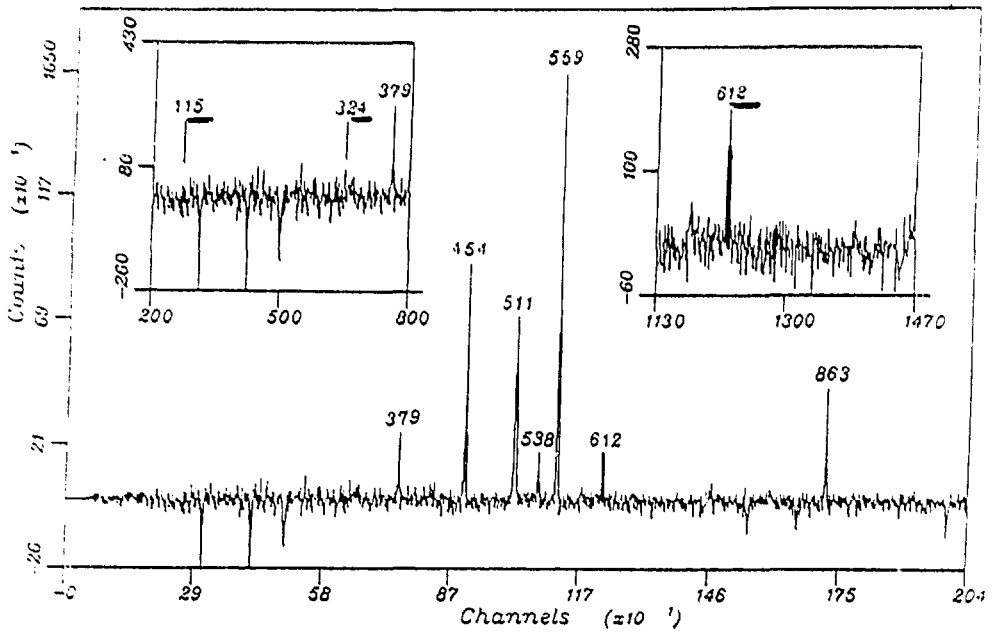

Fig. 10 The gamma rays in coincidence with the 709 keV line which is the 2-0⁺ transition in ^{72}Kr. The transitions not in ^{72}Kr are in ^{72}Se from a 709 keV transition in that nucleus.

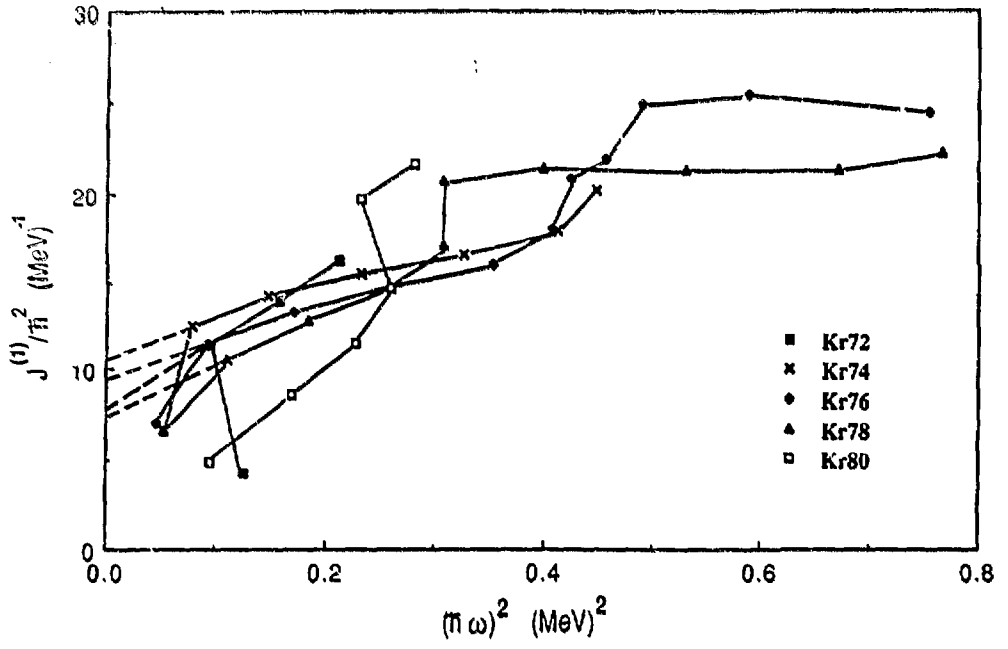

Fig. 11. Moments of inertia vs. $(\hbar\omega)^2$ for $^{72-80}$Kr (Dejbakhsh et al., 1990).

Other calculations (Åberg 1990) predict that the reinforcement of favored neutron and proton shell gaps could lead to superdeformation with $\beta_2 \sim 0.6$ (2:1 axis ratios) at low spin in $^{86}_{44}$Ru and perhaps in $^{80}_{30}$Zn. To study such exotic shapes which are likely to have low population in already very weak reaction channels will require higher efficiency RMS's than currently available and very efficient gamma-ray detector arrays. Thus, to observe the predicted different shape coexisting excited bands in these new N = Z nuclei and to extend the N = Z line, one must have a RMS with high rigidity to handle inverse reactions for a wide range of projectile-target combinations, not just a few, to allow both Z and mass identification, higher collection efficiency as well as a large solid angle and space for large detector arrays to make feasible RM-γ-γ and RM-Z-γ-γ coincidence studies.

A final note on the reinforcing and switching of shell gaps in nuclei comes from recent calculations of exotic cluster-decays for ^{78}Sr and ^{80}Zr by Gupta et al., (in press). One of the exciting discoveries of the last decade was the new form of radioactivity, heavy cluster decays such as ^{14}C and heavier, as predicted by Sandulescu, Poenaru, and Greiner (1980) Gupta et al., (in press) calculated the probabilities for cluster decays of $^{78}_{38}Sr_{40}$ and $^{80}_{40}Zr_{40}$. To illustrate the results, the emission of ^{24}Mg and ^{28}Si clusters have decay constants of (2.6×10^{-113}, 3×10^{-117}) and (2×10^{-54}; 1.8×10^{-56}) for ^{80}Zr and ^{78}Sr, respectively. So, ^{78}Sr is over fifty orders of magnitude more stable! These calculations provide further evidence for the reinforcing proton-neutron shell effect and switch in importance from the spherical 40 to the superdeformed 38 shell gap.

A NEW GENERATION RMS FOR HHIRF

The first in-beam gamma-ray studies in which a recoil mass spectrometer was used to mass gate the gamma spectra were reported (Hamilton 1984) from our work at the University of Rochester RMS. The Daresbury RMS began operation soon after. As noted above, research at Rochester and Daresbury in the mass 70 region have shown that it is absolutely essential to use inverse reactions in order to obtain Z in addition to mass identification of γ rays from unknown nuclei produced far off stability with very low cross-sections compared to other equal mass products. A new generation recoil mass spectrometer has been designed (Cormier et al., 1990) for use especially in inverse reactions with the Holifield Heavy Ion Research Facility accelerators with the following key characteristics:

a) High RMS rigidity; E/q ~ 15 MeV/q, to match to the beams at HHIRF for all inverse reactions,
b) Large 15 msr solid angle,
c) Large 75cm distance from target and focal plane to the first RMS element,
d) High quality beam rejection (10^{13}) far (~10m) from the target and focal plane,
e) High mass resolution, m/Δm ~ 1200, and
f) Flexibility to cover a broad range of present and future research.

The advantages of inverse reactions include, a) Z identification, b) kinematic focusing of the products into the RMS to improve RM-γ-γ rates factors of 5 to 500, c) allow alpha channels to be studied [alpha evaporation randomly kicks the recoils out of the RMS entrance in a normal reaction], and d) the recoils have energies (3-6 MeV/A) sufficient for radioactive beam experiments on secondary targets.

The RMS is illustrated in Fig. 12 in a new HHIRF addition. The major new features that make this a new generation RMS are its high rigidity, 15 MeV/q compared to 9 MeV/q in current systems and the momentum achromat between the target and the traditional components of an RMS. The importance of the high rigidity, 15 MeV/q compared to 9 MeV/q, to open up a wide range of inverse reactions is seen in Fig. 13. The achromat (with two dipoles seen on the left of Fig. 12) is the difference that opens-up inverse reactions with its intermediate focus where the beam is rejected. In a typical Rochester RMS with only electrostatic and magnetic deflection as in the right half of our RMS in Fig. 12, the primary beam will be passed with the similar energy reaction products in an inverse reaction of heavy projectiles on a light target. So, in a traditional RMS the products are orders of magnitude too weak to be seen in an inverse reaction. In the new design the beam rejection is far (>10m) from the counting areas around both the target and focal plane to significantly lower the background in large detector arrays when placed at these positions as shown in Fig. 12. The 75cm distances (target to first RMS element and last RMS element to focal plane) allow the 20 Ge detector HHIRF compact ball or 105 of the 110 Ge detectors for proposed arrays like GAMMASPHERE, a BaF_2 wall or other combinations around the target or focal plane.

As seen in Fig. 14, the mass resolution, m/Δm, of our RMS is 1000 to 1200, factors of 3 to 4 times greater than those at Daresbury, Argonne, and elsewhere. This much greater mass resolution makes a very significant improvement in eliminating at the focal plane the tails from adjacent masses with 10^3-10^4 larger cross-sections than the very low cross-sections of the products one wants to study, as occurs along the N = Z line. By using wire sources for a special case where a particular mass is critical for testing mass formulas, one could achieve a mass resolution of 10,000 with this RMS to provide an accurate direct mass measurement.

The improvements of RM-γ-γ triple coincidence counting rates of our RMS with the HHIRF 20 Ge detector close packed ball for normal and inverse reactions are illustrated in Table 3. Note the counting rates in the inverse (heavy ion beams) reactions are 6 to 39 times higher than in the normal (light ion beams) ones there, and this ratio can go up to factor of 500 in other cases. Such enhancement factors

can be the difference in doing and not doing an experiment. Even for the normal reactions (^{44}Ca beam), the RM-γ-γ rate for our system with 20 detectors (as in Table 3), would require 7d to collect 10^6 events but would require times of 58 and 31 days for 30 detectors at the Daresbury RMS and 14 in the Argonne RMS, respectively. So, even with a normal reaction, RM-γ-γ coincidence experiments are not feasible at these two facilities now.

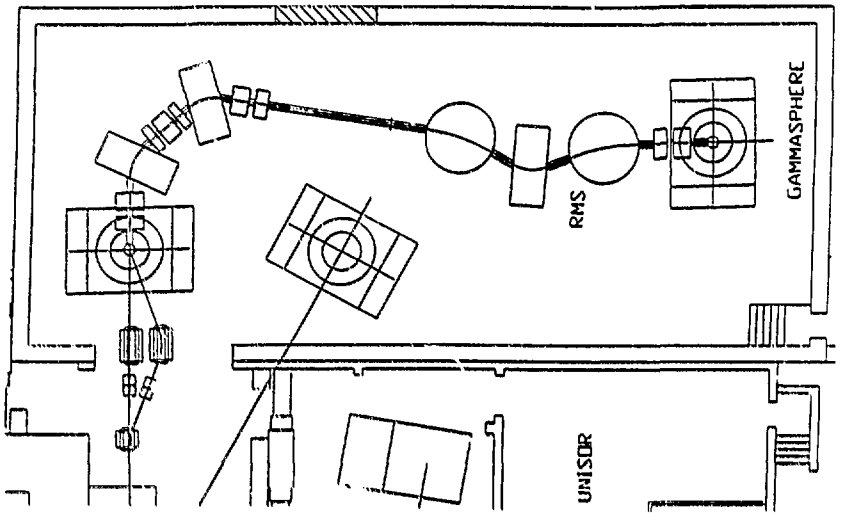

Fig. 12. New generation RMS for HHIRF. Target and achromat components are at the left and electrostatic (circles) and magnetic deflectors at the right.

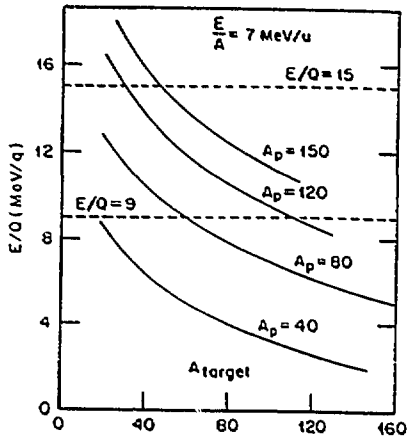

Fig. 13. Electrical rigidity vs. target A for different projectiles.

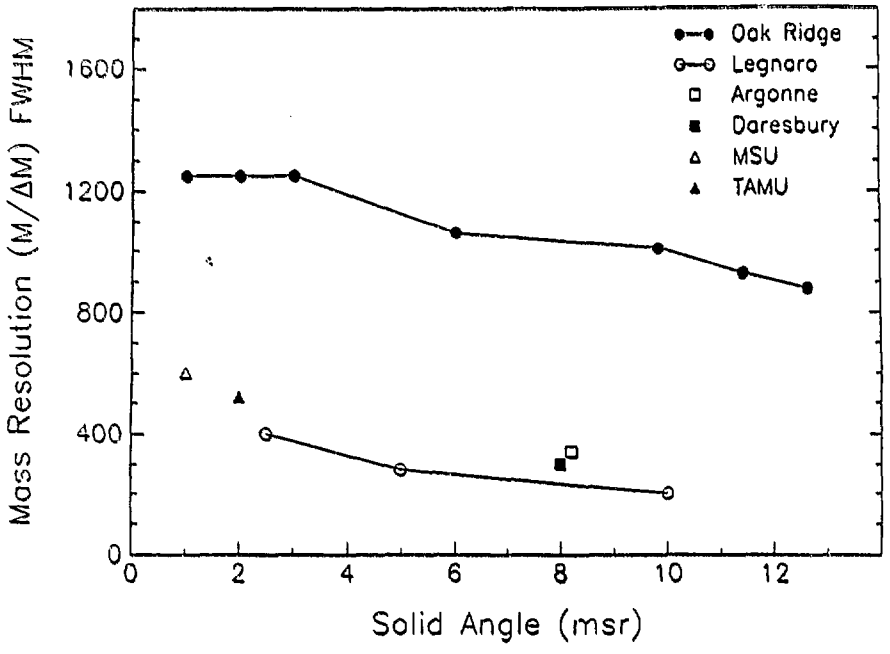

Fig. 14. Mass resolutions of existing and proposed RMS's are compared.

Table 3. Normal and inverse reactions at 5 MeV/A beam energies are compared for 8 msr RMS solid angle.

	$^{44}Ca + ^{122}Sn$		$^{32}S + ^{154}Gd$	
	Normal	Inverse	Normal	Inverse
E/Q (MeV/q)[a]	2.5	10.2	1.7	12.8
E/Q (MeV/Nucleon)[a]	0.4	2.7	0.2	3.6
Recoil Mass-γ-γ[b]	1,700	10,000	440	17,000

[a]The values are for the compound nucleus. [b]For 20 Compton suppressed Ge detectors, 12 cm from the target and E_γ = 1 MeV.

Our new RMS with the present 20 Ge detector ball will open up RM-γ-γ coincidences of recently identified N = Z nuclei like ^{68}Se to ^{80}Zr to definitively establish their level structures which are based currently only on singles data, except for ^{72}Kr as discussed above. In each of these N = Z nuclei, we can significantly improve the statistics including ^{84}Mo where only one γ ray was weakly observed. In ^{84}Mo it should be easy to observe the additional levels necessary to definitively establish the deformation of its ground state and test the importance of the N=Z = 42 shell gaps. Also, we expect to establish better the structures and pin down whether there are

low-lying, competing near-spherical bands in ^{76}Sr and ^{80}Zr which interact with their superdeformed ground states as has been suggested occurs by analogy to the mass 100 region based on their energy level spacings (Hamilton 1989; Hamilton 1990). We also should establish the competing structure in ^{72}Kr. Finally, the greatly improved counting statistics will open up studies of a few more N = Z nuclei with higher Z, including a search for an excited superdeformed band ($\beta_2 \sim 0.6$) predicted in ^{88}Ru.

To definitively establish the neutron and proton single particle orbitals and their interaction along the N = Z line, one must study nuclei to either side of the N = Z line. Here the real power of our RMS with a large array like GAMMASPHERE is demonstrated. For example, consider seeking to identify the new $T_Z = -1$ $^{70}_{36}Kr_{34}$ nucleus with two neutrons less than N = Z. In the reaction $^{16}O(^{58}Ni,4n)^{70}_{36}Kr_{34}$ with 290 MeV ^{58}Ni, the ^{70}Kr count rate is 500 times greater in our RMS in the inverted reaction compared to the normal (^{16}O beam) reaction for a given beam intensity. For a total reaction cross-section of 1.1b, 1mg/cm^2 target, 10pnA beam and singles count rate of 40kHz in 105 Ge detectors, we estimate at the end of a 3-day run 60 counts in a specific gamma ray in ^{70}Kr, produced with σ = 10nb, when gated by another gamma ray and mass! A RM-γ-γ coincidence experiment on an isotope with 10^{-8} production of the total. Present in-beam γ-γ coincidence spectroscopy studies of nuclei far from stability are prohibitive for production rates of 10^{-3}-10^{-4} of the total. This represents an astonishing increase in sensitivity to study new, very far off stability nuclei of factors up to 10^4 to 10^5!

Using inverse reactions and our RMS alone, one can produce radioactive beams with sufficient energies, 3-5 MeV/A (see Table 3) to do Coulomb excitation of the radioactive secondary beam and to do compound nuclear reactions on secondary targets. By bombarding ^{44}Ca with ^{122}Sn, Coulomb excitation of the ^{160}Yb product could yield B(E2)'s to the 2^+, 4^+ states in a few hours (recall ^{168}Yb is the lightest Coulomb excited Yb). As another example consider a ^{116}Sn beam on a ^{12}C target to produce ^{124}Ba (^{130}Ba is the lightest stable barium isotope) with 5 MeV/u. At this energy a stable ^{124}Ba can undergo a second reaction on ^{12}C to produce ^{132}Nd + 2p2n (^{142}Nd is the lightest stable Nd isotope).

A RADIOACTIVE BEAM FACILITY AND RMS AT HHIRF AND THE N = Z LINE

Recent international conferences at Berkeley, Los Alamos and Belgium have drawn worldwide attention to the fascinating new physics to be opened up by a facility which can provide a wide range of beams of radioactive nuclei with sufficient energies and intensities to study compound nuclear, transfer, capture, and Coulomb excitation reactions. Numbers of proposals are being made to add a second accelerator and a mass separator coupled to an existing accelerator. Fortunately, HHIRF already has two accelerators and sufficiently well shielded space between them where the accelerators can be coupled through a mass-separator-ion-source as shown in Fig. 15 to give 95 different radioactive beams from ^{6}He to ^{84}Rb with energies up to 5 to 13 MeV/A and intensities 10^6 to 10^{10} ions/s at very modest cost of $3-4 million in less than 2 years. This facility could produce across the periodic table over 200 compound nuclei which cannot be produced by any combination of stable target and stable beam. This is illustrated for one region of the periodic table in Fig. 16. A brief description of the HHIRF proposal for an Oak Ridge Exotic Beam (OREB) extension is given to indicate the exciting capabilities this facility offers (Garrett and Olsen 1991).

Beams of H, d, ^{3}He, ^{6,7}Li and ^{10,11}B would be accelerated in the cyclotron and strike a target in the shielded room. There, the products would be mass separated, and a low energy negative-ion output provided to the tandem. The first easy beams would be ^{14,15}O, ^{17,18}F, ^{29,30}P, ^{30,31}S, $^{68-74,76}$As, and $^{70-72}$Se with 10^9-10^{10} ions/s intensities.

The radioactive beam facility at HHIRF has definite advantages (in addition to very low cost) over all other currently proposed light ion drivers and high energy heavy ion fragmentation facilities. In the former group, all the others proposed have a

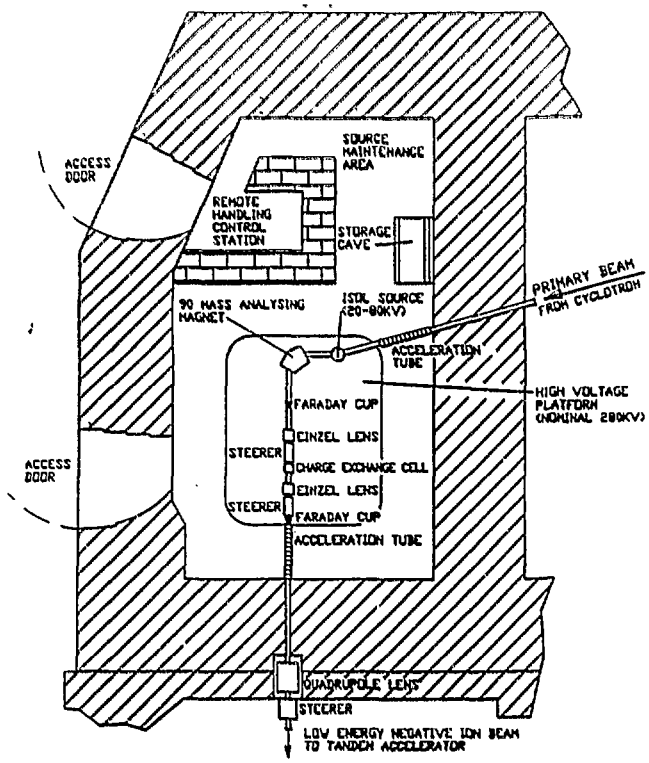

Fig. 15. Plan view of target room C111 showing details of the proposed radioactive beam facility high-voltage platform and source maintenance area.

mass range <60 and with one exception low energies of ≤1.5 MeV/A. In the fragmentation reactions, the energies of the fragments are so high, 50-500 MeV/A, that they are too energetic for many nuclear structure and astrophysics studies. For some problems storage rings can be used, but then short lifetime products are lost and internal targets which limit detection or re-acceleration are required. In principle, the new GSI SIS-18 with storage ring can be used for some such experiments but in practice this is a costly way to use a machine designed for high energy, heavy ion research.

Many new, presently unknown isotopes from A ~ 50 to 250 can be produced in quantities sufficient to carry out nuclear structure studies with the HHIRF radioactive beam facility that cannot be studied with stable beams and targets. These new isotopes offer many exciting and presently inaccessible opportunities to test in very stringent ways under new extreme conditions of the N/Z ratio the microscopic independent-particle quantum structure that forms the foundation of the nuclear shell model, the behavior of identical proton and neutron high j orbitals and the proton-neutron interaction, theoretical predictions of new regions of exotic nuclear shapes, nuclear mass formulas, and the proton drip line.

The importance of the N = Z nuclei was discussed earlier. Recall, the heaviest N = Z nucleus $^{84}_{42}Mo$ was only identified in 1991 and there only one γ ray, presumably the 2^+-0 transition, was seen (Gelletly et al., 1991). A long-sought goal to test the spherical shell model under new extremes in the ratio of the Coulomb to nuclear force has been to study $^{100}_{50}Sn_{50}$ which should be spherical double magic. Recall, based on spherical double magic $^{68}_{28}Ni_{40}$ and $^{90}_{40}Zr_{50}$, one would have expected $^{80}_{40}Zr_{40}$ to be spherical

for if a rather high m number of configurations would be constructed. An improved variational scheme which incorporates such correlations in a systematic way, no matter where in energy they occur, is done in the new excited FED (from few determinant VAMPIR) approach (Schmid et al., 1989). Starting with the VAMPIR solution which is not taken out of the variational space, one instead looks first for a second symmetry-projected determinant correlating this solution in a variational calculation. Then, a third determinant is constructed, and so forth, up to n_1 configurations. The resulting correlated yrast state is then eliminated from the variational space, and the procedure is repeated to construct the first excited state with the same symmetry, and so on, through the m lowest states (each now being a linear combination of several configurations). Finally, as in excited VAMPIR, the now much smaller residual interaction is diagonalized. This procedure has the big advantage that the dominant correlations on top of the projected mean-field solutions are accounted for in each state separately.

This new method was applied to the high-spin states in ^{68}Ge (Chaturvedi et al., 1991). The theoretical states are grouped into several bands in Fig. 19. Some changes do occur at the higher spins compared to the excited VAMPIR calculation (Petrovici et al., 1989), and a new band with superdeformation, $\beta \sim 0.42$, labeled in Fig. 19, now appears. The new excited FED VAMPIR results are compared with our new experimental data for the high-spin, positive-parity bands in ^{68}Ge by renormalizing the theoretical spectrum to the experimental 2_1^+ level as shown in Fig. 19. The main features are summarized below. The experimental bands are ordered from left to right according to the theoretical predictions in Fig. 19.

Up to angular momentum 6^+ the calculated yrast levels are almost pure oblate states. The theoretical g factor for the 6_1^+ is 0.37 while the experimental (Barclay et al. 1986) value is 0.4. The oblate band then continues where the 8_2^+ (with an oblate component of about 85%) most probably is the 8_3^+ state of the experimental spectrum. The 10_3^+ state has a pure oblate nature to form an oblate band, labeled by "O" in Fig. 19, that continues, as indicated by the older excited VAMPIR results, up to rather high angular momenta.

Besides this oblate structure, four other distinct bands are obtained in the calculations. They are all prolate deformed but differ in the magnitude of their quadrupole and hexadecapole moments as well as in their pairing properties. They also display different alignments. The band labeled as "ν-al" is characterized by an almost empty $0g_{9/2}$ proton level while the neutrons in the same shell-model orbit contribute to it a considerable portion of its total angular momentum. This strong neutron alignment is reflected in the small g factors of the members of this band: -0.03 for the theoretical 8_3^+ band head of the ν-al band. The 8_3^+ level and its ν-al band likely correspond to the experimental 8_2^+ 5051 keV level, which has a measured (Barclay et al., 1986) g factor of -0.28 ± 0.14 and the band built on it. The two bands labeled as "D" and "S" have almost the same quadrupole deformation on the neutron side; however, on the proton side, the latter band is considerably more deformed. This is evident from the intrinsic quadrupole moments ($\beta_2 \sim 0.42$ as compared to ~0.34) of the leading configuration as well as from the B(E2) values, which above spin 12 are about twice as large in the "S" band as in the "D" band. Note, the predicted new "S" band with a large moment of inertia agrees quite well with the new experimental band shown on the far right. The "D" band and the $18_2^+ \rightarrow 16_2^+ \rightarrow 14_2^+$ sequence, labeled as "Y", are probably associated with one of the experimental bands shown directly above the ground band 0-2-4 sequence. The calculated $18_1^+ \rightarrow 16_1^+ \rightarrow 14_1^+$ decay path is rather slow (mainly because of the small transition energies) and, thus, this path is unlikely to be seen in the experimental data.

All these prolate bands discussed in the last section have one common feature: their members become strongly mixed as soon as spin values as low as 12^+ or 14^+ are reached. Consequently, there are many competing decay branches for the various 14^+, 12^+, 10^+, and even 8^+ states. Thus, the decay does not run only via stretched E2 transitions within the various bands but also via a few strong $\Delta I = 0$,M1 transitions (indicated

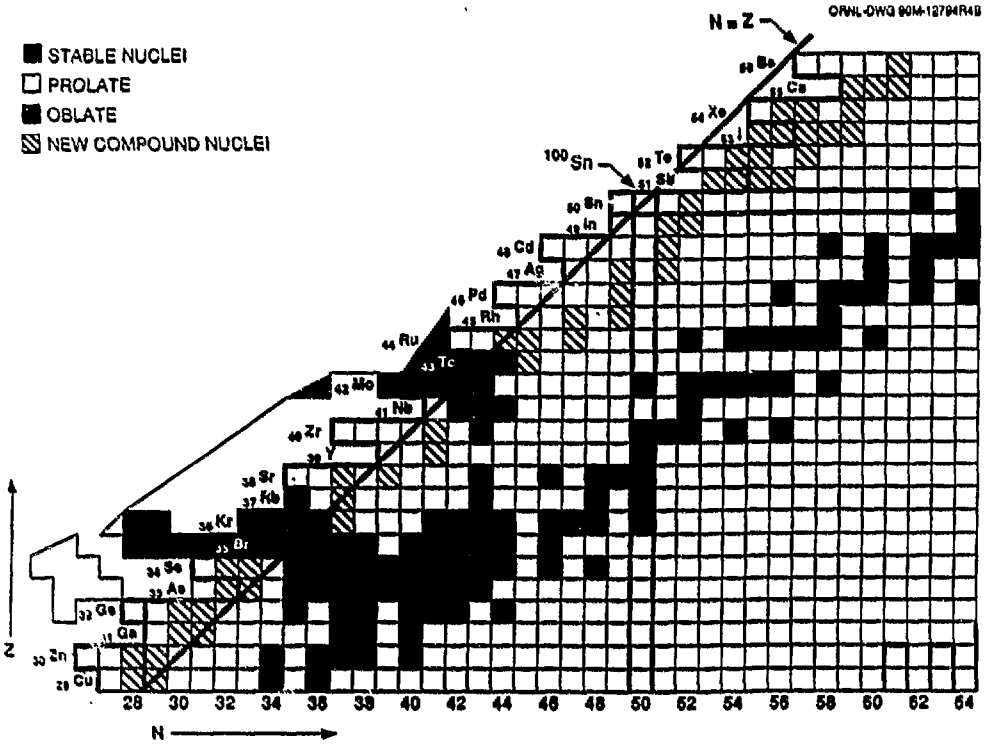

Fig. 16. The "new" proton-rich compound nuclei Z = 29-56 that can be produced by the proposed exotic beam extension of the Holifield Facility and cannot be produced by combinations of stable beams and targets are denoted by the shaded squares (Garrett and Olsen, 1991). For comparison, the regions of proton-rich nuclei in which the nuclear ground state is predicted (Moller and Nix, 1981) to be deformed ($\varepsilon_2 > 0.20$ or < -0.20) are indicated by gray denoting oblate deformation with the isotopes between the two gray areas out to the drip line being prolate, respectively. Stable nuclei are shown as solid squares and the proton and neutron closed shells and drip lines are indicated by heavy lines. Likewise the line of self-conjugate nuclei (N=Z) is indicated as is the location of the doubly closed shell nucleus ^{100}Sn.

double magic, but it has one of the most deformed ground states ($\beta_2 \sim 0.4$) known. The lightest tin isotope that has been studied experimentally is ^{103}Sn (Tidemand-Pedersson et al., 1981). So far, efforts to identify ^{102}Sn have been unsuccessful.

The problem is that the most proton-rich compound system at or above Z = 50 that can be formed using stable beams has $T_z = 2$. So, at least four neutrons must be evaporated to reach ^{100}Sn. Since charged-particle emission dominates so far off stability, a 4n process has a vanishing small cross section. However, the OREB with ^{68}As and ^{70}Se beams would allow $T_z = 1$ compound systems to be formed, and these would require the emission of only two neutrons to populate ^{100}Sn, eg. ^{40}Ca(^{70}Se,2α2n)^{100}Sn or the reaction ^{39}K(^{68}As, α3n)^{100}Sn. These cross sections are estimated to be the order of a few microbarns, similar to that of ^{84}Mo (7 ± 3 μb) for the 2n channel. The Daresbury RMS and detectors used to identify ^{84}Mo are much less efficient than our proposed RMS with our 20 Ge detector closed-packed ball.

With beams of ^{68}As and ^{70}Se, the estimated cross sections for the production of nuclei surrounding ^{100}Sn are of the order of 1.0 mb for ^{101,102}Sn, 0.3 mb for ^{99}In, 7.0 mb for ^{100}In, and 0.2 mb for ^{103}Sb (Garrett and Olsen, 1991). The predicted cross section for ^{101}Sn is enhanced by nearly two orders of magnitude relative to the largest cross sections available with stable beams. Calculations also indicate that the singly-magic nuclei (N = 50, Z = 46-48) and (Z = 50, N > 53) have cross sections greater than 10 mb. Therefore, an experimental program based on ^{68}As and ^{70}Se beams would allow (Garrett and Olsen, 1991):

1) the determination of single-particle and single-hole energy levels around the ^{100}Sn doubly closed shell;

2) the extraction of many empirical two-body residual interactions involving these states;

3) the measurement of masses of a large number of nuclei near ^{100}Sn; and

4) detailed spectroscopic information for the Sn isotopes above mass 100.

The ^{100}Sn single-particle and single-hole energy levels are crucial information needed to constrain the parameters of various nuclear models.

Let me emphasize studies along the N = Z line and other very low cross section products will only be possible if the radioactive beam facility has a high rigidity, recoil mass spectrometer capable of handling inverse reactions such as our new generation RMS just described.

An area that is closely related to the studies of the N = Z line is the understanding of the proton-neutron interaction. It is known that the isoscalar residual interaction between neutrons and protons provides an understanding of nuclear deformation. Federman and Pittel (1979) building on the work of de Shalit and Goldhaber (1953) and Talmi (1962) stressed that when shell effects are important, the occupation of neutrons and protons in spin orbit partner orbitals plays an important role. The strong overlap between the neutron and proton orbits, especially when $n_n = n_p$ and $\ell_n = \ell_p$ provides the opportunity for strong interaction. This is itself a reinforcement between neutrons and protons. Federman and Pittel (1979) used this approach to describe the sudden onset of deformation around ^{100}Zr. As noted earlier (Hamilton 1989), however, it is not clear how this picture can encompass the ^{98,100}Sr superdeformation and the superdeformation around ^{76}Sr. Much too little is known about the pn interaction in those regions. The radioactive beam facility at ORNL will enable one to study many of the self-conjugate nuclei in the mass 80 and 130 regions where the partner orbitals can be important.

Another major driving force behind the development of radioactive beam facilities is to study many inaccessible questions in nucleosynthesis (Garrett and Olsen, 1991). At high densities and temperature, nuclear reactions can compete with beta decay. Such conditions characterize nuclear burning and nucleosynthesis in a variety of sites including the early universe, matter accreting neutron stars and supernova. Existing nucleosynthesis models rely on reaction rates, masses, level densities, isomeric states, and nuclear shapes all of which are unknown for nearly all the far

off stability nuclei. In the absence of experimental data on these parameters, theoretical estimates must be used in the calculations. For example, the existence of isomers is ignored and shapes are expected to be quite different in many cases from the spherical shapes used in calculations. With radioactive beams, we can measure these properties for many currently inaccessible exotic nuclei across the periodic table for input in nuclear astrophysics, nuclear structure and nuclear mass calculations.

Energy generation in the hot CNO cycle (Fig. 17) is limited by beta decay at $^{14,15}O$. At temperatures near 0.5×10^9 °K the beta sequences can be bypassed by the sequences $^{14}O(\alpha,p)^{17}F(p,\gamma)^{18}Ne(\beta)^{18}F(p,\alpha)^{15}O$. At higher T the $^{15}O(\alpha,\gamma)^{19}Ne$ and $^{18}F(p,\gamma)^{19}Ne$ reactions open up the break-out reaction $^{19}Ne(p,\gamma)^{20}Na$ and the hydrogen driving rp-process to give a hundredfold increase in the power of the hot CNO cycle (Kubono et al., 1981; Wiescher et al., 1986). The HHIRF RIB facility OREB could give a complete characterization of all but the ^{19}Ne reaction. With the RMS one can obtain a unique characterization of these reactions by gating on the recoil product of interest. A massive white dwarf accreting matter from a proton-rich companion star could lead to a thermonuclear explosion on the white dwarf (as shown in Fig. 18) or likewise in a neutron star. In these areas, rapid proton burning, the so-called rp-process, can proceed to mass 80 or 100. The path of the rp-process again is determined by the balance between beta decay and the reaction rates for large densities of "high-energy" protons. This path follows just those proton-rich nuclei that become accessible to study using the proton-rich radioactive beams at OREB (HHIRF). In the rp-process, reaction rates of the heavier proton-rich nuclei are unknown as well as their nuclear structure. Again, many of these studies will involve inverse reactions requiring our new RMS. The proposed HHIRF radioactive beam facility would open up the study of the proton-rich part of three of the four major areas identified in the report of the nuclear astrophysics working group at the recent Workshop on the Science of Intense Radioactive Beams (Howard et al., 1990), namely: a) nuclear capture reactions involving stellar processes, b) production of exotic nuclei for r-process and rp-process modeling, c) nuclear transfer reactions for simulating specific neutron, proton, or alpha capture reactions (Garrett and Olsen, 1991).

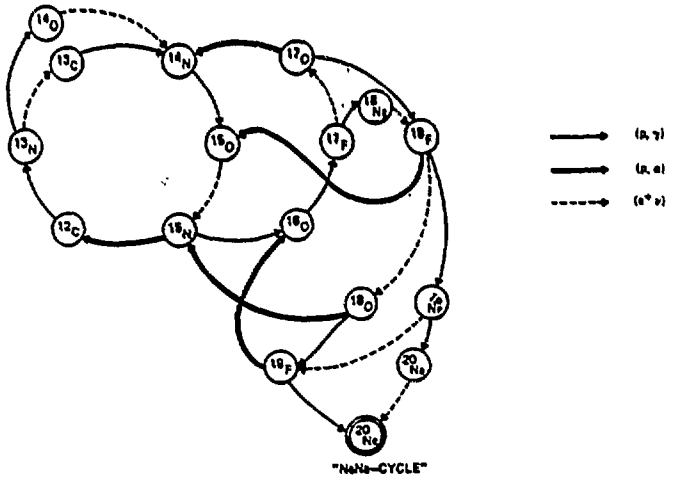

Fig. 17. Schematic figure of hydrogen burning in the 'hot" CNO cycle taken from Rolfs and Rodney (1988). Two of the four exotic nuclei (^{13}N, ^{17}F, ^{18}F, and ^{19}Fe) for which proton-induced reactions are proposed, ^{17}F and ^{18}F, can be accelerated by the proposed extension to the HHIRF. Likewise, alpha-particle-induced "breakout" on ^{14}O and ^{15}O also can be studied (Garrett and Olsen, 1991).

Fig. 1b ...graphical conception of the cataclysmic binary star system ... Aquarii in which matter extracted from a red giant accumulates in an accretion disk around a white-dwarf companion until it deto... nates in a thermonuclear explosion. The disk channels the debris of the resulting nova into a long, narrow jet. This is shown in the inset which is a recent Hubble Space Telescope enhanced photograph sensitive to the light of doubly-ionized oxygen. The jets, corresponding to an explosion thought to have occurred in the late 1970s, can be traced over ... $\times 10^{13}$ km. The binary itself is contained within the dark blotches at the center of the nebulosity. This figure is taken from the January 1991 issue of Sky and Telescope and is used with permission of Sky and Telescope and Francesco Paresce of the Space Telescope Science Institute (Garlett and Olsen, 1991)

...ESULTS OF MICROSCOPIC CALCULATIONS IN THE A = ... REGION

...the multiplicity of structures and their rapid changes with N and Z make the A = ... region an important testing ground of nuclear models (Hamilton et al., 1986). The existence of overlapping bands built on different nuclear shapes was discovered (Hamilton et al., 1974) in $^{72}_{34}Se_{38}$ where the low-lying excited band has ... and the ... band ... as discussed. The coexistence is related to the competition between the shell gaps at very large prolate superdeformation ... and the ... gaps at ... (Hamilton et al., 1986). The ...

the near spherical nucleus $^{68}_{32}Ge_{36}$ triple forks at 8^+ into three bands with no crossing transitions observed earlier (de Lima et al., 1979, 1981). The g-factor measurements in ^{68}Ge support the interpretation that the two lowest 8^+ bands are aligned neutron configurations, and the third band is a continuation of the ground state (Barclay et al., 1986).

One of the important challenges in nuclear physics is to develop more microscopic models which can predict the excited energy levels of nuclei. With the various shape coexisting structures seen in the mass-70 region, these nuclei provide stringent challenges for microscopic theories. Recently, a microscopic investigation of the low-spin states in ^{68}Ge and ^{72}Se has been made by using a self-consistent description of the nuclear excitation by a Hartree-Fock-Bogoliubov-based theory with spin and number projection before the variation, the excited VAMPIR approach (variation after mean-field projection in realistic model space [Petrovici et al., 1989]). These calculations predicted a much more complex level structure for ^{68}Ge including strong M1 transitions crossing between the three known bands beginning at 8^+ and between new bands. A similar complex band structure is predicted in ^{72}Se, but such complex structures were not observed in recent work (Mylaeus et al., 1989).

We reinvestigated both ^{68}Ge and ^{72}Se with the spin spectrometer and the closed-packed Ge ball at HHIRF (Holifield Heavy Ion research Facility) to study their high-spin structures which provide important tests of the new microscopic calculations. In ^{68}Ge new bands and mixing of bands are observed, but not in ^{72}Se (Chaturvedi et al., 1991). New microscopic calculations were carried out for ^{68}Ge and ^{72}Se in an improved excited few determinant VAMPIR approach which has been developed recently and applied to sd-shell nuclei (Schmid et al., 1989).

In ^{68}Ge, 19 new levels were observed experimentally including two new bands, as shown in Fig. 19. The new band beginning with the 12^+ 7561-keV level goes up to the highest spin observed. New crossing transitions between the known bands and the new bands also are observed. More importantly, the new band beginning at 7561-keV has a moment of inertia that is considerably larger than that of the previously known one shown next to it as can be seen by comparing their energies of the similar spin transitions in the two bands. Only the positive-parity bands are shown in Fig. 19.

On the other hand, careful searches revealed no new positive parity band structures in ^{72}Se (Fig. 20). Note in Fig. 20 the experimental 0^+ ground state and the 2^+_1 state are members of the ground-state band with small oblate deformation. The observed 0^+_2 and 2^+_2 deformed states are not shown. There is mixing of the near spherical oblate and very large prolate deformed bands in the 2^+, 4^+ and 6^+ levels. Discrete γ-ray transitions were observed above 18^+ up to 26^+. The high-spin states in ^{72}Se are dominated by a single cascade as shown in Figs. 3, 20. The negative-parity bands, which are only seen at lower spins, are not shown. The static and dynamic moments of inertia of ^{72}Se are remarkably constant and large, approaching the rigid-body value at higher spins.

The complex experimental bands encountered in ^{68}Ge call for a model in which all the essential degrees of freedom are taken into account in a completely microscopic fashion and not put in case-by-case. These should include the coexistence of different shapes and other collective phenomena as well as the various alignments and other single-particle excitations. One way to construct such a model is the use of variational techniques, as is done in the various approaches of the so-called VAMPIR (variation after mean-field projection in realistic model spaces) family (Schmid and Grümmer 1987 and references therein; Schmid et al., 1989 and references therein). However, by introducing only one additional determinant for each new state to be considered, this approach is still a type of mean-field approximation and may not always be sufficient, since the residual interaction between the lowest m configurations does not necessarily account for the dominant correlations on top of each of the various excited VAMPIR solutions. Often (Schmid and Grümmer 1987) the dominant correlations, for example, to the yrast solution are related to rather high-lying configurations. Within the excited VAMPIR approximation such could only be accounted

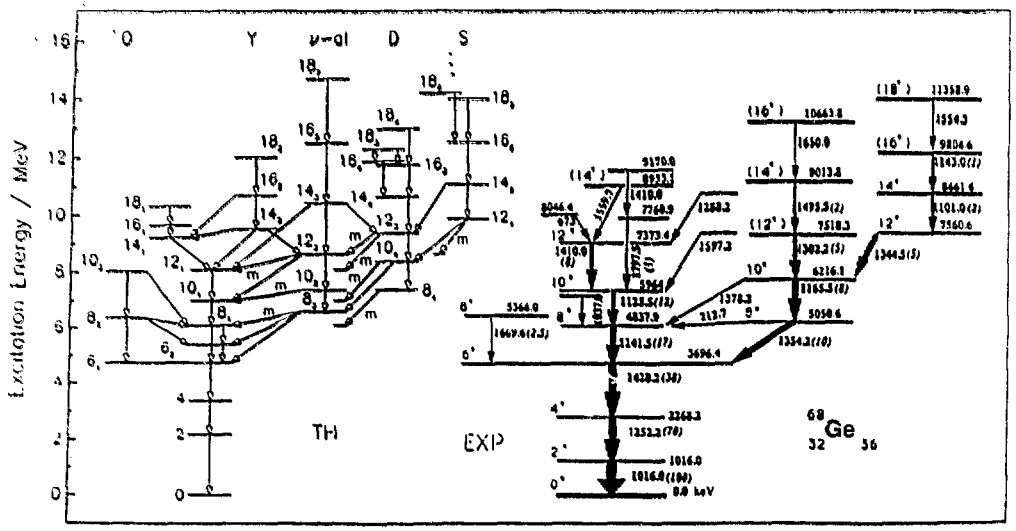

Fig. 19 Positive-parity levels in ^{68}Ge. On the left are the levels calculated in the FED VAMPIR approach. The symbols 0, γ, ν-al, D, and S used to identify the bands are described in the text. The continuation of the oblate ground band is seen on the left and a new superdeformed prolate ($\beta \sim 0.42$) band is shown on the right in the calculation. The experimental levels reported here are shown on the right-hand side of the picture. The experimental bands are ordered (oblate on the left, superdeformed on the right) to match up with the calculated levels on the left side and matching the observed properties (lifetimes, magnetic moments, and moments of inertia) of each band with the calculated properties of each band. The D band in the calculations may be the new band which feeds the 5963-keV 0$^+$ level (Chaturvedi et al., 1991).

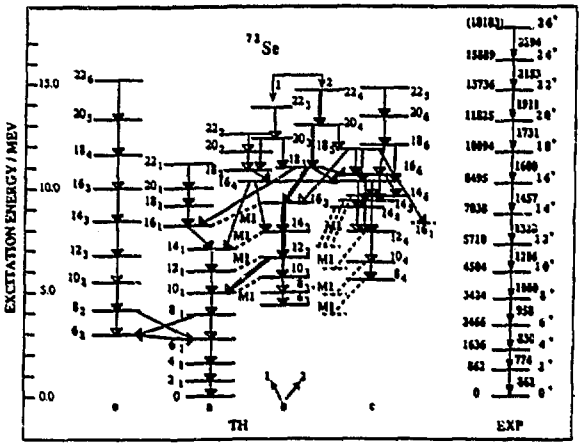

Fig. 20. Positive parity levels calculated and observed in ^{72}Se (Chaturvedi et al., 1991). A fast E2 path in the calculation is shown by double lines.

by "a" on the figure) which mainly feed the yrast band at these angular momenta. Such crossing transitions are now seen in the experimental data, too. Similar large B(M1) transitions are also predicted in between some of the higher states. The theoretical results are strongly supported by the observation of not only several 8^+, but also several energetically bunched 10^+, 12^+, and 14^+ states in the new data with crossing transitions and the new "S" band with much larger deformation.

Similar new theoretical calculations were carried out for ^{72}Se, and the results are shown in Fig. 20. The theoretical complex positive-parity-energy level spectrum looks rather similar to that of ^{68}Ge and is in sharp contrast to the single positive parity yrast band seen experimentally (Fig. 20) to high spin. Any crossing transition to other bands predicted in the calculations has an experimental branching intensity less than 10% of the observed cascade feedings at any level. However, a detailed look at the calculations reveals that there is a path of predicted very fast cascade E2 transitions (noted in Fig. 20) which cross from one band to another with large deformation, with only slow (weak) transitions to other states. It is possible that the experimental yrast band seen to high spins is a composite of several bands all with quite large deformation and linked by a very fast E2 path, as indicated in Fig. 20. On the other hand, the experimental levels may be only a single band with superdeformation that simply dominates the experimental spectra because the lower energies of its members provide the fastest decay path.

In summary, the detailed agreement between the new microscopic excited FED VAMPIR calculations and the new experimental structures observed in ^{68}Ge are quite striking for such complex multiple shape coexisting structures. This agreement in such a complex nucleus provides strong encouragement for the development of realistic microscopic models. On the other hand, the new calculations indicate similar complex structures for ^{72}Se, but in sharp contrast to ^{68}Ge the ^{72}Se experimental high-spin positive parity states are surprisingly dominated by a single band. This strong confirmation of the microscopic calculations in ^{68}Ge and marked differences in ^{72}Se are a clear challenge. It is possible that this difference is related to the fact that $^{72}_{34}Se_{38}$ is much closer to the new island of ground state superdeformation centered around N = Z = 38 (Hamilton 1989) and that the dominance of these reinforcing proton and neutron shell gaps at 38 is not included in the calculations yet.

E0 TRANSITIONS BETWEEN SHAPE COEXISTING STRUCTURES IN MASS 120 REGION

Mantica et al. (1990) have studied with the UNISOR isotope separator the levels of ^{120}Xe and compared its structure to the even-even Xe isotopes below N = 82 and to the N = 66 mid-shell isotones above and below the Z = 50 closed shell. They note that the odd-mass nuclides in this region have low energy "intruder" $9/2^+$ states that have been attributed to the promotion of a proton from below the Z = 50 shell gap with the promoted proton paired with the "normal" $g_{7/2}$ or $d_{5/2}$ configuration to yield a $g_{9/2}^{-1}$ hole state. The mean square charge radii of the Xe nuclides show a gradual increase in deformation in going from N = 82 to mid-shell at N = 66 with $\beta_2 = 0.3$ for ^{120}Xe, for an axially-symmetric shape. The 2_1^+ energies in the even-even Xe nuclei decrease smoothly from both sides toward a minimum in mid-shell N = 66 ^{120}Xe.

Just as in the region of Pt-Hg and the Z = 82 shell closure, the promotion of two protons across the Z = 50 proton shell closure can yield a relatively low energy 0^+ excited state or even ground state in even-even nuclei, especially around N = mid-shell. This coexisting intruder state should have a quite different radius compared to the normal proton configuration. While γ decay is forbidden between the 0^+ intruder and 0^+ normal states, E0 internal conversion electron radiation whose strength is proportional to the difference in their nuclear radii, can be strong. Such E0 transitions also may occur in any $\Delta I = 0$ transition between bands built on the two different shapes. No evidence for enhanced E0 strength in $^{124-128}$Xe has been found (Walters et al., 1988; Mantica et al., 1989; Ohya et al., 1980). The N = 66 mid-shell nucleus, $^{120}_{54}Xe_{66}$, has been investigated extensively at UNISOR by internal conversion and γ-ray studies. Careful measurements of the internal conversion

coefficients in the UNISOR work revealed six pure E0($0^+ \rightarrow 0^+$) transitions and four $\Delta I = 0$, E0 enhanced transitions in ^{120}Xe in sharp contrast with $^{124-128}$Xe. The levels of ^{120}Xe are shown in Fig. 21 where ΔI=0 transitions with enhanced E0 strength, and 0-0 transitions are shown by heavier lines. These levels are best described by a deformed ground band and γ vibrational band (on the right in Fig. 21) with 2^+_γ at 876 keV with the same radius and a near-spherical excited band with one- and two-phonon-vibrational states built on it as shown on the left in Fig. 21. The strong E0 transitions occur between those bands which have different radii but not between the γ and ground band, where there is essentially no change in root mean square radius. The absence of E0 radiation in transitions between the γ-vibrational and ground bands which have similar RMS radii and their presence in transitions between β-vibrational and ground bands which have different RMS radii is well-known in rare earth nuclei (Hamilton 1972a,b).

The levels of $^{120}_{60}Xe_{60}$ are just reversed from what is found in spherical closed shell Z = 50, $^{118}_{50}Sn_{68}$ (Brun et al., 1979) where the ground band is spherical, and a low-lying excited band is well deformed (Fig. 22). Similar structures to ^{120}Xe, though somewhat distorted, are found in ^{118,122}Xe. The N = 66 isotones (Fig. 22) show a remarkable symmetry around N = 50 where the deformed band is very high in energy (1757 keV) dropping to 1135 keV in $^{114}_{48}$Cd and 951 in $^{118}_{52}$Te, then becoming the ground state of $^{112}_{46}$Pd and $^{120}_{54}$Xe with the onset of well-deformed structures for Z = 56, 58 and 44, 42. This is an additional region where a systematic pattern of shape coexisting structure around a major closed shell is becoming clearly defined.

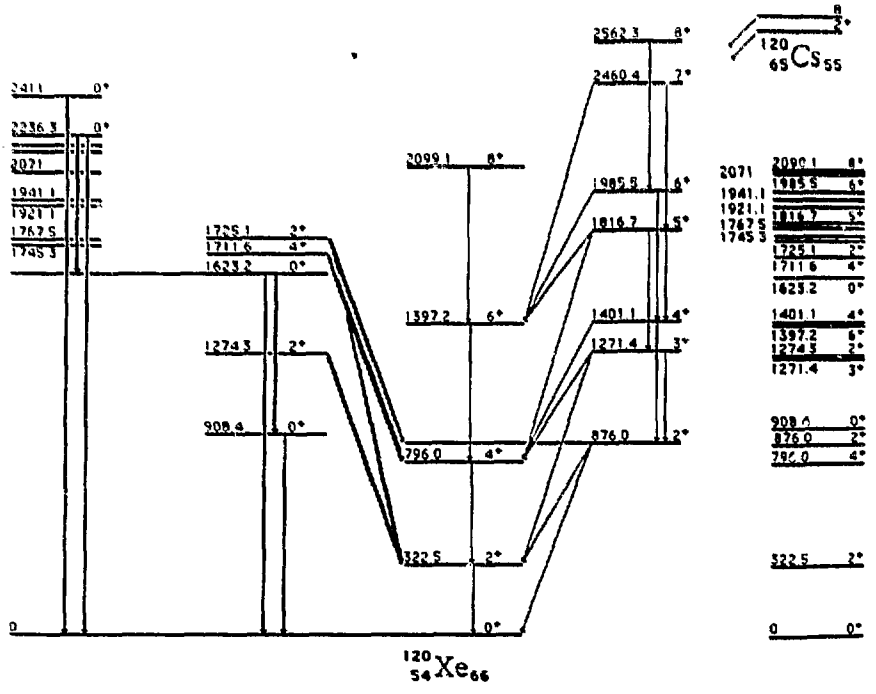

Fig. 21. ^{120}Xe levels with only selected γ-ray transitions are shown. Heavy lines indicate the presence of E0 radiation (Mantica et al., 1990).

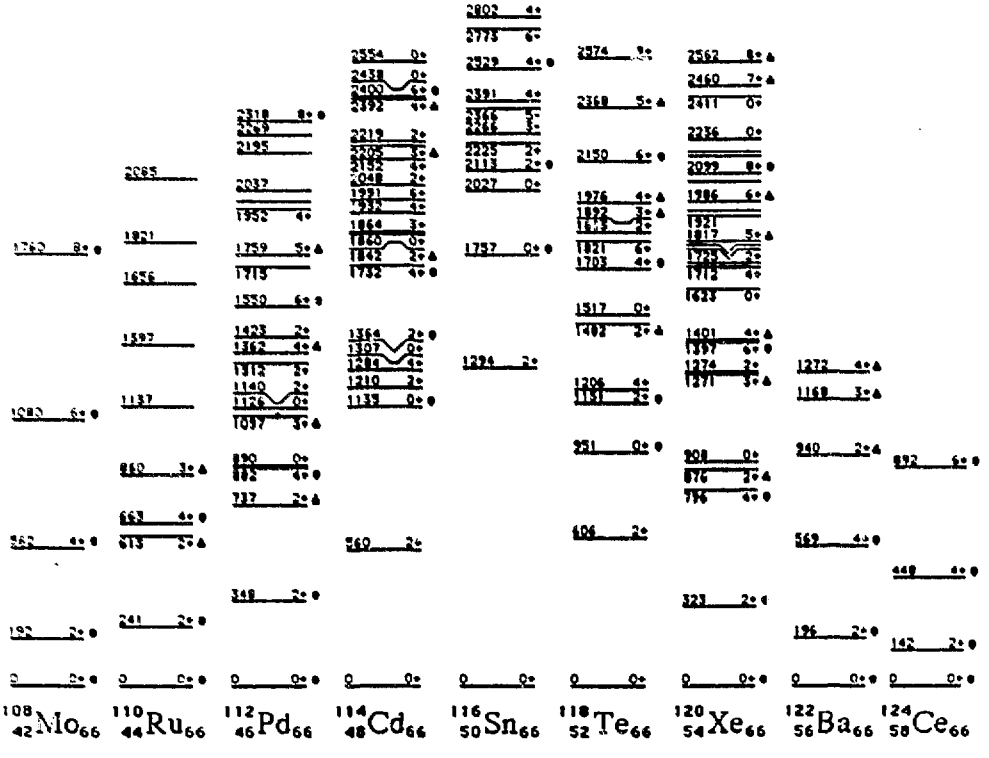

Fig. 22. Systematics of the N=66 isotones near the Z=50 closed shell. The dots indicate deformed states and the triangles γ-band states.

VARIETIES OF SHAPE COEXISTENCE IN MASS 180-190 NUCLEI

The region bounded by 78 ≤ Z≤ 82, 104 ≤ N ≤ 114 was one of the first regions where shape coexistence was established (Hamilton et al., 1975, 1976) and continues as the most fertile ground known for the studies of multiple coexistence of different shapes, intruder orbitals, electric monopole transitions, superdeformation and other phenomena. Here, I select only a few recent highlights. The even-even $^{184-188}$Hg isotopes were the first classic examples of nuclear shape coexistence where full bands of levels were seen above and below the crossing of their near-spherical ground states and well-deformed shapes. As seen in Fig. 23, in-beam studies by our group and the Canberra group have traced the band head of the excited deformed potential minimum through its energy minimum and subsequent rise at lower N in ^{180,182}Hg.

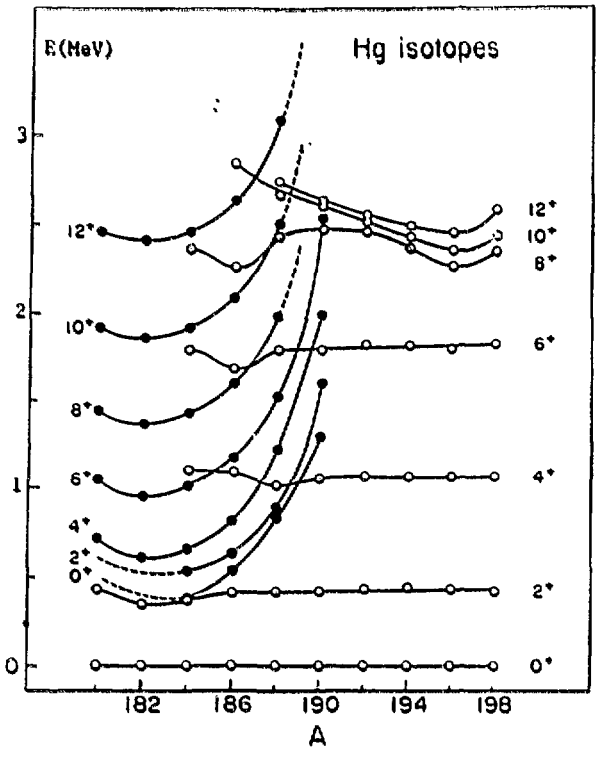

Fig. 23. The systematics (Hamilton 1989) of strongly-deformed bands (filled circles) and weakly-deformed bands (open circles) in the even-mass Hg isotopes.

In total routhian surface (TRS) calculations with a Woods-Saxon potential, the shape coexistence observed in $^{182-188}$Hg was predicted to disappear in ^{190}Hg, eg. there would be no excited normal prolate band with $\beta_2 \sim 0.2$ deformation (Bengtsson et al., 1987) as seen in Fig. 24. However, recent UNISOR work (Kortelahti et al., 1991) located in ^{190}Hg an excited deformed band (see Fig. 25) which has risen higher in energy in line with what one might expect from the extension of the lower mass data as shown in Fig. 23. However, this excited deformed band has considerably smaller deformation, $\beta \sim 0.14$, than that ($\beta_2 \sim 0.24$) of the excited bands in $^{182-188}$Hg. On the other hand, these calculations (Bengtsson et al., 1987a) do predict the superdeformed minimum at $\beta_2 \sim 0.45$, which is observed experimentally. These data, coupled with the superdeformation discovered at moderately higher spins in ^{190}Hg demonstrate the complexity of competing shapes relatively near the ground state in this region. Naturally it is important for a full understanding of these nuclei that theoretical calculations predict the normal deformed prolate band in ^{190}Hg as well as the more near spherical ground state and superdeformation at higher excitation. New potential energy surfaces have been calculated for $^{184-190}$Hg in terms of the Nilsson-Strutinsky method with a standard κ, μ parameter set and a modified set. Now it is found that there is a low-lying, second minimum in the potential energy on the prolate side in addition to the known oblate minimum (Fig. 26) (Zhang and Hamilton, 1991). The existence of such a prolate minimum, which is not found in recent total routhian surface calculations, offers an explanation of the recent observation of an excited deformed band in ^{190}Hg. The calculated deformation of the minimum, $\epsilon_2 = 0.12$, is consistent with the new experimental one in ^{190}Hg. Our calculations reproduce the

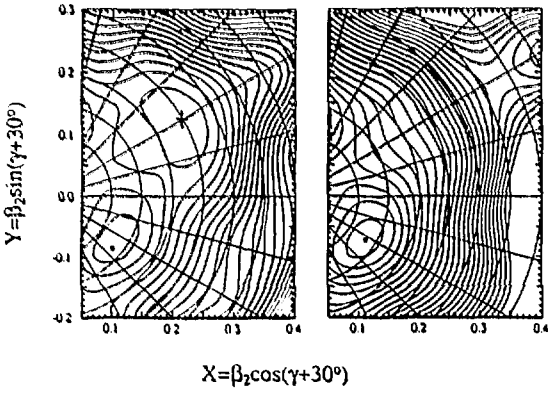

Fig. 24. Total routhian surface calculations with a Woods-Saxon potential at $\hbar\omega$ = 0.05 MeV (Zhang 1987; Bengtsson et al., 1987; Bengtsson and Nazarewicz, 1987b). The prolate minimum is marked by a cross in (a) for ^{184}Hg, but this prolate minimum is not seen in (b) for ^{190}Hg.

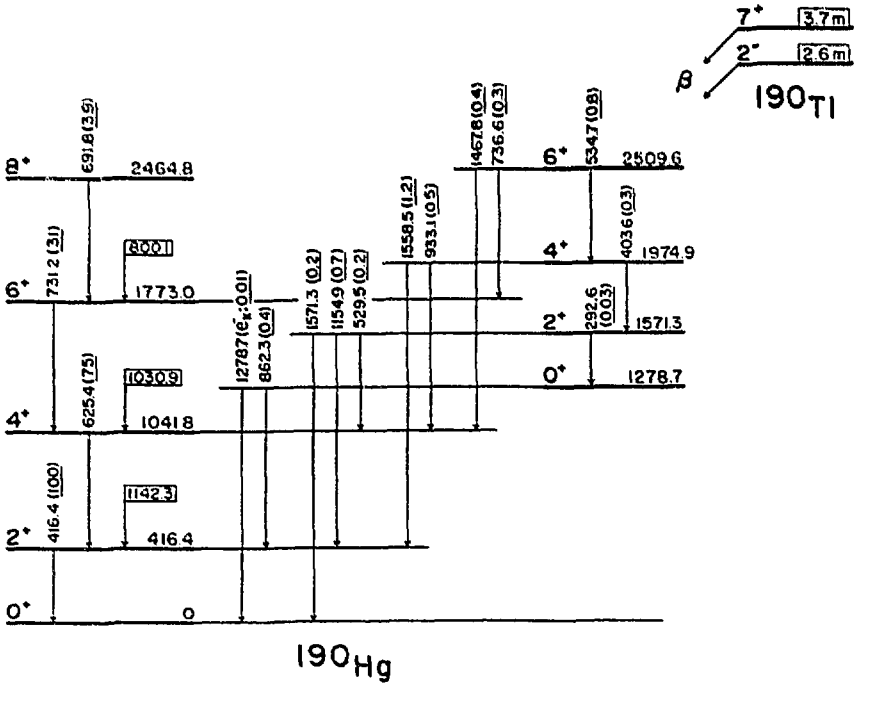

Fig. 25. Part of the level scheme of ^{190}Hg populated in the β^+/EC decays of ^{190m,g}Tl. Energies are in keV and γ-ray transition intensities are given relative to $I\gamma(416) = 100$. The 1279 keV transition is pure E0 and, thus, only its K conversion electron intensity is given.

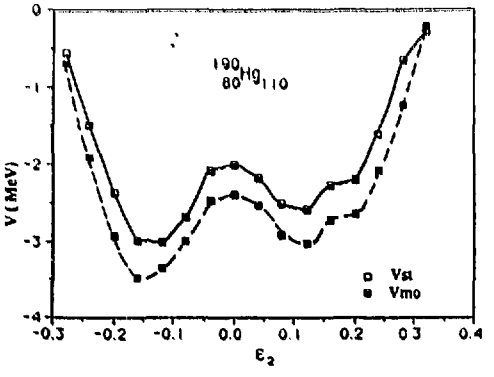

Fig. 26. The potential energy V vs. quadrupole deformation ϵ_2 curve for the nucleus ^{190}Hg. The solid line is obtained with a standard κ, μ parameter set, while the dashed line was obtained with a modified one (Zhang and Hamilton, 1991).

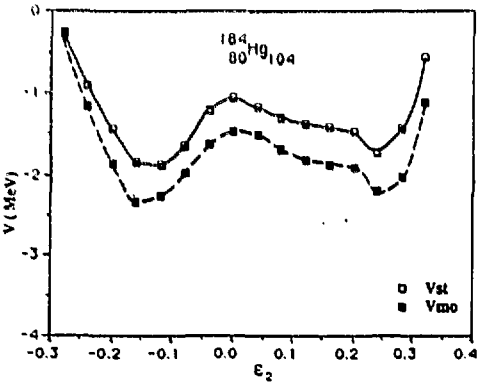

Fig. 27. The same as Fig. 26 for the nucleus ^{184}Hg (Zhang and Hamilton, 1991).

sharp decrease in the excited deformed band in ^{190}Hg compared to the same bands in $^{184-188}$Hg. The calculations for $^{184-188}$Hg are illustrated in Fig. 27. It is not strange to find such a deformation jump in the prolate minima in going from N < 110 to N = 110. In fact, one can easily see from the Nilsson diagram that, for small prolate deformation (ϵ_2 about 0.1), the high K (up-sloping) orbitals of $h_{9/2}$ and $i_{13/2}$ will be met when N is equal to and larger than 110. However, for N < 110, there are several high j, low K (down-sloping) orbitals, and even more than that, there are gaps in the single particle spectrum on the prolate side with $\epsilon_2 \geq 0.2$ for N = 102, 104, 106 and 108. Therefore the fact that a prolate minimum with a smaller ϵ_2 value shows up on the potential energy surface of ^{190}Hg is quite reasonable.

One of the signatures of the shape coexisting structures in this region is the enhanced E0 transitions in $\Delta I = 0$ and $0^+ \rightarrow 0^+$ transitions. Zganjar and Wood (1990) recently reviewed the UNISOR work in which a remarkable richness of E0 transitions

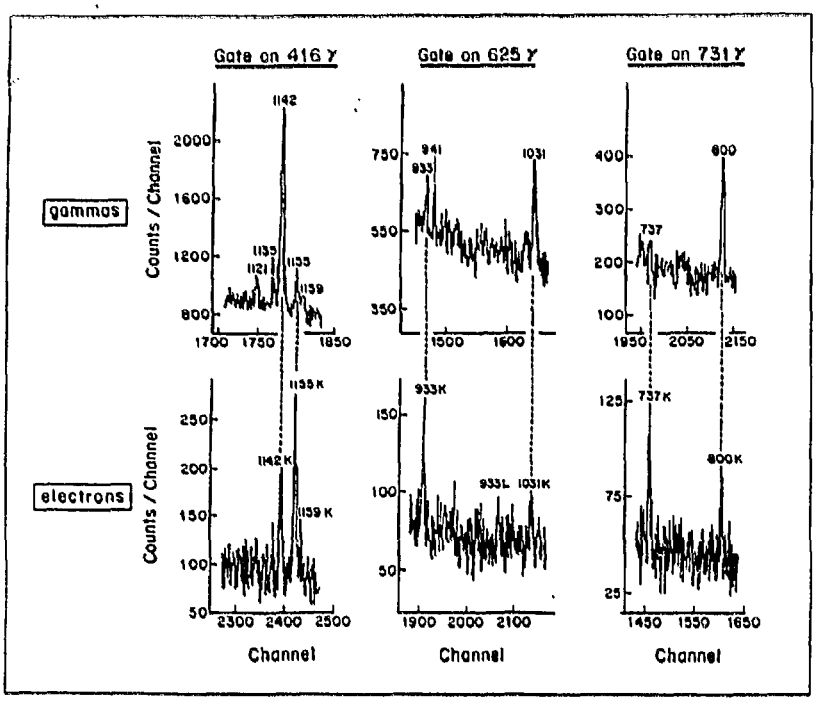

Fig. 28. Portions of the gamma-ray and conversion-electron spectra in coincidence with the $2^+ \rightarrow 0^+(416)$, $4^+ \rightarrow 2^+(626)$, and $6^+ \rightarrow 4^+(731)$ γ-ray transitions in the ground-state band of ^{190}Hg. The 800, 1031, and 1142 keV transitions (E2 or M1+E2) are shown for comparison with the very-converted 1155, 933, and 737 keV transitions.

has been observed in this region, including for the first time the establishment of E0's in odd-A nuclei. Earlier, four different shape coexisting structures were observed in ^{185,187}Au connected by enhanced E0 transitions. These four different structures are formed by coupling proton hole states to the two shape coexisting structures in ^{186,188}Hg and particle states to different shape coexisting structures in ^{184,186}Pt (Papanicolopulos et al. 1988). Summarizing their work, they have identified very converted transitions (VCTs) ($\alpha_K >> \alpha_K$ M1 or E2) in the following nuclei: two VCTs in ^{195}Pb (Griffin 1987), ten VCTs in ^{185}Pt (Schwarzenbert et al., 1988), and three VCTs in ^{193}Pt (Schwarzenberg et al., 1989) (for example, see Fig. 28). Even more astonishing, they find (Krane et al., 1991; Schwarzenberg et al., 1988) several transitions in ^{185}Pt and one in ^{184}Pt for which only conversion electrons are observed in a cascade of transitions -- no gamma rays are seen! This is an unprecedented phenomenon in nuclei for $I^\pi \rightarrow I^\pi$ transitions with $I \neq 0$. The observation of such transitions could call into question in-beam γ-ray studies which would not observe the E0 strength and so completely miss one or more transitions when they are dominated by E0 radiation. Finally, their study of ^{181}Pt (Schwarzenberg et al. 1991, in progress) has not yielded any VCTs. This is seen to be consistent with a shape coexisting, band-crossing hypothesis in which an intruder band, formed from the promotion of pairs of protons from above the Z = 82 shell, drops down and crosses the normal ground state. The entire collection of low-energy, low-lying, odd-mass VCTs are shown in Fig. 29. The figure also displays the lowest known excited 0^+ states across the mass surface. The $176 \leq A \leq 187$ region obviously exhibits a distinct correlation between low-lying excited 0^+ states and low-lying VCTs in odd-mass

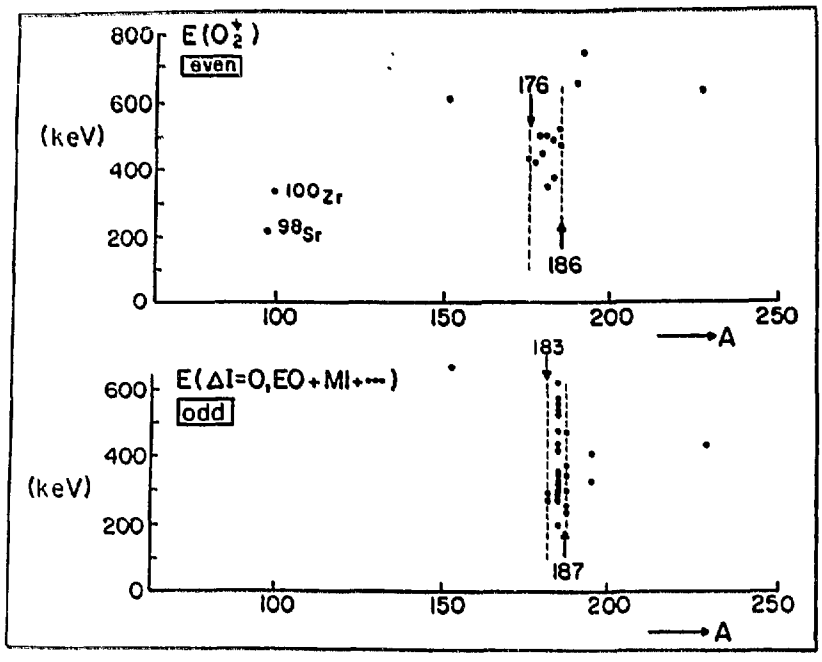

Fig. 29. The energy of 0_2^+ states in even-even nuclei below about 800 keV (upper part) and the energy of transitions in odd-mass nuclei which have large E0 components (lower part). The data (Zganjar and Wood, 1988; and recent UNISOR results) represent nearly all known cases of E0 enhanced transitions in odd-mass nuclei at these low energies.

nuclei. The VCTs are interpreted as resulting from electric monopole transitions between shape coexisting structures which mix. In the Pt isotopes the effect is dramatic because of the crossing (Zganjar and Wood 1990) of the coexisting band heads near A = 186 where the $h_{9/2}$ intruder is shown to penetrate and fall below the normal ground state for A = 187 to 177. Mixing between the bands formed on these states would result in an abundance of E0 transitions in ^{187}Pt and ^{185}Pt at the crossing, diminishing for ^{183}Pt, and reappearing at the very light end of this isotope chain, probably near ^{178}Pt. The ten VCTs observed in ^{185}Pt, three in ^{183}Pt, and none in ^{181}Pt are consistent with this picture. Obviously, there is still much experimental and theoretical work to be done to understand all the varieties of shape coexistence being observed.

ACKNOWLEDGEMENTS

Work was supported in part by the U.S. Department of Energy under Grants DE-FG05-88ER40407 and DE-AC05-76OR00033 at Vanderbilt University and UNISOR, respectively.

REFERENCES

Åberg, S. (1990). In: Nuclear Structure in the Nineties (Noah R. Johnson, ed.), Vol. I, North-Holland, Amsterdam, in Nucl. Phys., A520, 35c.

Azuma, R. F., et al. (1979). Phys. Lett., 86B, 5.

Barclay, M., et al. (1986). J. Phys. G Lett., 12, L295.

Bengtsson, R., et al. (1987a). Phys. Lett. B., 183, 1.

Bengtsson, R. and W. Nazarewicz (1987b). In: Proc. Int. Conf. on Nuclear Shapes: The Variety of Nuclear Shapes (J. D. Garrett, et al., eds.), p. 371, World Scientific, Singapore.

Bergstrom, I. (1966). Nucl. Inst. Methods, 43, 116 and 119.

Bjørnholm, S. and J. E. Lynn (1982). Rev. Mod. Phys., 52, 725.

Bron, J., et al., (1979). Nucl. Phys., A318, 335.

Chaturvedi, L., et al. (1991). Phys. Rev. C, 43, 2541.

Cormier, T., et al. (1990). Nucl. Instr. and Meth. in Phys. Res., A297, 199.

de Shalit, A. and M. Goldhaber (1953). Phys. Rev., 92, 1211.

de Lima, A. P., et al. (1979). Phys. Letts., 83B, 43.

de Lima, A. P., et al. (1981). Phys. Rev. C., 23, 213.

Dejbakhsh, H., et al. (1990). Phys. Lett., 249, 195.

Federman, P. and S. Pittel (1979). Phys. Rev., C20, 820.

Garrett, J. D. and D. K. Olsen (1991). Editors of: A proposal for physics with exotic beams at the Holifield Heavy Ion Research Facility, Physics Division/ORNL, Oak Ridge.

Gelletly, W., et al. (1991). Phys. LEtt., 253B, 289.

Girod, M., et al. (1990). In: Nuclear Structure in the Nineties (Noah R. Johnson, ed.), Vol. I, p. 93, North-Holland, Amsterdam.

Gorres, J., et al. (1987). Phys. Rev. Lett., 58, 662.

Griffin, J. C. (1987). Ph.D., Georgia Tech. and work in progress.

Gupta, R. K., W. Scheid and W. Greiner (in press).

Hamilton, J. H. (1972a). Izv. Akad Nauk. USSR Ser. Fiz., 36, 14

Hamilton, J. H. (1972b). In: Int. School on Nuclear Structure (V. G. Soloviev, ed.), p. 332, Joint Inst. for Nuclear Structure, Dubna.

Hamilton, J. H., et al. (1974). Phys. Rev. Lett., 32, 239.

Hamilton, J. H., et al. (1975). Phys. Rev. Letts., 35, 562.

Hamilton, J. H., et al. (1976a). Phys. Rev. Lett., 36, 340.

Hamilton, J. H., et al. (1976b). In: Proc. Int. Conf. on Selected Topics in Nuclear Physics, Vol. II (V. G. Soloviev, et al., eds.), p. 303.

Hamilton, J. H. (1981). In: Int. Symp. on Nuclear Collectivity (A. Arima and T. Marumori, eds.), p. 87, INS, Tokyo.

Hamilton, J. H. (1984). In: Proc. Fifth Adriatic Int. Conf. on Nuclear Physics, in Fundamental Problems in Heavy Ion Collisions (N. Cindro, et al., eds.), p. 111, World Scientific, Singapore.

Hamilton, J. H. (1985a). In: Proc. Int. Symp. on Nuclear Shell Models (M. Vallieres and B. H. Wildenthal, eds.), p. 31, World Scientific, Singapore.

Hamilton, J. H. (1985b). In: Nucleus-Nucleus Collisions from the Coulomb Barrier Up to the Quark-Gluon Plasma (A. Faessler, ed.), p. 107, Pergamon Press, New York.

Hamilton, J. H. (1989). In: Treatise on Heavy Ion Science, Vol. VIII (A. Bromley, ed.), p. 21, Plenum Press, New York.

Hamilton, J. H. (1990). In: Nuclear Structure in the Nineties (Noak R. Johnson, ed.), North-Holland, Amsterdam, in Nucl. Phys., A520, 377c.

Hamilton, J. H. (1991). In: Int. Conf. on Nuclear Shapes and Nuclear Structure at Low Excitation Energies, in press.

Howard, W. M. et al. (1990). Report from Working Group 3: Nuclear Astrophysics. In: Proc. of the Workshop onthe Science of Intense Radioactive IOn Beams (J. B. McClelland and D. J. Vieira, eds.), p. 68, Los Alamos National Lab Report LA-11964-C.

Jansen, Robert V. F. and Teng Lek Khoo (1991). Annu. Rev. Nucl. Part. Science, 41, 321.

Kahn, T. A., et al. (1977). Z. Phys., A283, 103.

Kirwan, A. J., et al. (1987). Phys. Rev. Lett., 58, 467.

Kortelahti, M. O., et al. (1991). Phys. Rev. C, 43, 484.
Krane, K. S. and UNISOR Collaborators (1991). Work in progress.
Kubono, S., et al. (1981). Ap. J., 344, 460.
Lister, C. J., et al. (1987). Phys. Rev. Lett., 59, 1270.
Lister, C. J., et al. (1988). In: AIP Conf. Proc. 164: Nuclei Far From Stability, IV Int. Conf. (I. S. Towner, ed.), p. 354, AIP, New York.
Mantica, P. F., et al. (1990). In: Exotic Nuclear Spectroscopy (W. C. M°Harris, ed.), p. 495, Plenum Press, New York.
Moller, P. and J. R. Nix (1981a). Nucl. Phys., A301, 199.
Moller, P. and J. R. Nix (1981b). At. Data Nucl. Data Tables, 267, 165.
Mylaeus, T., et al. (1989). J. Phys. G, 15, L131.
Nazarewicz, W., et al. (1985). Nucl. Phys., A503, 285.
Ooi, S. S. L. (1986). Phys. Rev., C34, 1157.
Ohya, S., et al. (1980). INS Tokyo Prog. Rept. 40.
Petrovici, A., et al. (1989). Nucl. Phys., A504, 277.
Piercey, R. B., et al. (1981). Phys. Rev. Lett., 47, 1514.
Riley, M. A., et al. (1990). Nucl. Phys., A512, 178.
Rolfs, C. E. and W. S. Rodney (1988). Caldrons in the Cosmos. Univ. Chicago Press, Chicago.
Sandulescu, A., et al. (1980). Sov. J. Part. Nucl., 11, 528.
Satteson, M., et al. (1990). J. Phys. G: Nucl. Part. Phys., 16, L27.
Schmid, K. W. and F. Grummer (1987). Rep. Prog. Phys. 50, 731.
Schmid, K. W., et al. (1989), Nucl. Phys. A499, 63.
Schwarzenberg, J., et al. (1988). Bull. Am. Phys. Soc., 33, 1603.
Schwarzenberg, J., et al. (1989). Bull. Am. Phys. Soc., 31, 1825.
Schwarzenberg, J., et al. (1991). Work in Progress.
Shirmer, J., et al. (1989). Phys. Rev. Lett., 63, 2196.
Strutinsky, V. M. (1967a). Ark. Fys., 36, 629.
Strutinsky, V. M. (1967b). Nucl. Phys., A95, 420.
Talmi, I. (1962). Rev. Mod. Phys., 34, 704.
Twin, P., et al. (1986). Phys. Rev. Lett., 57, 811.
Varley, B. J., et al. (1987). Phys. Lett., B193, 1463.
Walters, W. B., et al. (1988). Hyperfine Int., 43, 343.
Wiescher, M., et al. (1986). Astron. Astrophys., 160, 56.
Zganjar, E. F. and J. L. Wood (1988). In: Proc. workshop on Nuclear Structure in the Zirconium Region (J. Eberth, et al., eds.), p. 88, Springer Verlag, Berlin.
Zganjar, E. F. and J. L. Wood (1990). In: Nuclear Structure in the Nineties (Noah R. Johnson, ed.), North-Holland, Amsterdam, in Nucl. Phys. A520, 427c.
Zhang, Jing-Ye and J. H. Hamilton (1991). Phys. Letts. B, 260, 11.
Zhang, J.-Y. (1987). In: Proc. Conf. on Physics at Tandem (J. C. Jiang, et al., eds.). p. 512, World Scientific, Singapore.